Arabian Journal of Chemistry (2022) **15**, 104278

King Saud University

Arabian Journal of Chemistry

www.ksu.edu.sa
www.sciencedirect.com

ORIGINAL ARTICLE

The site preference and doping effect on mechanical properties of Ni_3Al-based γ′ phase in superalloys by combing first-principles calculations and thermodynamic model

Hamid Ali [a], Rong Chen [a], Bo Wu [a,b,*], Tianliang Xie [a], Liangji Weng [a], Jiansen Wen [a], Qipeng Yao [a], Longju Su [a], Yan Zhao [a], Panhong Zhao [b], Baisheng Sa [a], Yu Liu [c], Chunxu Wang [c], Hang Su [c], Asif Hayat [d,e,*]

[a] *Multiscale Computational Materials Facility, Key Laboratory of Eco-Materials Advanced Technology, College of Materials Science and Engineering, Fuzhou University, Fuzhou 350100, China*
[b] *Materials Design and Manufacture Simulation Facility, School of Advance Manufacturing, Fuzhou University, Jinjiang 362200, China*
[c] *Central Iron & Steel Research Institute Group, Beijing 100081, China*
[d] *College of Chemistry and Life Sciences, Zhejiang Normal University, Jinhua 321004, Zhejiang, China*
[e] *College of Geography and Environmental Sciences, Zhejiang Normal University, Jinhua 321004, China*

Received 23 May 2022; accepted 14 September 2022
Available online 21 September 2022

KEYWORDS

Ni-based superalloys;
Site preference;
Sublattice model;
Mechanical properties;
First-principles calculations;
Alloy thermodynamics

Abstract The fundamental aspects of site preference of alloying elements on sublattice of the strengthen γ′ phase with $L1_2$ structure have not been well understood, which hinders the optimized design of advanced Ni-based high-temperature alloys. In this contribution, the temperature- and composition-dependent site occupying preferences of the binary, ternary, and quaternary of Ni_3Al-based γ′ phase alloyed with M_i where M_i represents the additional transitional metals Co, Cr, Cu, Fe, Mn, Mo, Re, Ta, Ti, V, or W atoms (arranged in alphabetical order) chosen frequently, were studied using a two-sublattice thermodynamic model $(Ni, Al, M_i)_{1a}(Ni, Al, M_i)_{3c}$. The site occupying fractions (SOFs) were calculated based on a thermodynamic database established in this work, where the thermodynamic data of the end-members involved were obtained using first-principles calculations and phonon spectrum calculations. The calculated SOFs results show that there is an obvious site preference for stoichiometry binary Ni_3Al, and its site configuration changes

* Corresponding authors.
E-mail addresses: wubo@fzu.edu.cn (B. Wu), asifncp11@yahoo.com (A. Hayat).
Peer review under responsibility of King Saud University.

Production and hosting by Elsevier

https://doi.org/10.1016/j.arabjc.2022.104278

from $(Al)_{1a}(Ni)_{3c}$ at room temperature to $(Al_{0.9984}Ni_{0.0015})_{1a}$ $(Al_0Ni_{0.9994})_{3c}$ at 1273 K. For the γ′ phase with the composition 78Ni-26Al-4M_i (atom ratio and x_{Ni}/x_{Al} = 3:1), Mo atoms always preferred to occupy the 1a sublattice (Al site), Co, Mn, and Ti atoms always prefer the 3c sublattice (Ni site) in the whole temperature range, while the site preference of Cr, Cu, Fe, Re, Ta, V, or W atom is affected by temperature. For example, when the heat treatment temperature is lower than 700 K, Cr, Cu, Fe, Ta, V, and W atoms occupy the 1a and 3c sublattice randomly, and Re atoms prefer to 3c sublattice, while when the heat treatment temperature is higher than 1273 K, Cr, Cu, and W atoms prefer 3c sublattice, Fe and Ta atoms prefer to 1a sublattice, while all Re atoms occupy the 3c sublattice exclusively, and all V atoms occupy the 1a sublattice exclusively, respectively. Likewise, the site preference of the quaternary system with selective compositions 78Ni-26Al-2 M_1-2 M_2 was also predicted. Based on calculated SOFs results, the mechanical and thermodynamic properties were studied at the ground state. It has been revealed that Cr, Re, and V doping can improve the microhardness of Ni_3Al alloys; in particular, the effect of Cr is extraordinary; and all elements, except Mn, Mo, and Ti, would enhance the bulk modulus of Ni_3Al-based γ′ phase, in which Mn have the greatest influence on reducing the bulk and shear modulus, respectively. Furthermore, all the B/G ratios of the computed Ni_3Al-based γ′ phase are >1.75, showing inherent ductility. Only Cr doping significantly enhances the Debye temperature of the Ni_3Al-based γ′ phase.

1. Introduction

Since their discovery in the 1940 s, Nickel-based superalloys have got significant importance for the design of high-temperature applications such as modern turbine engines, nuclear power, chemical processing plants, and rocket engines based on their outstanding characteristics i.e., corrosion-resistant behaviors, lightweight, and excellent mechanical properties (Brimhall et al., 1983; Hung et al., 1983; Ivanov et al., 1988; Miracle and No, 1993; Noebe et al., 1993; Inoue et al., 1998; Golberg et al., 1999; Lu and Hirohashi, 1999; Pal et al., 2006; Pollock and Tin, 2006; Reed, 2006; Darolia et al., 1993). The γ′-Ni_3Al intermetallic compound is incredibly important in science and technology due to its effective high-temperature oxidation resistance and exceptional high-temperature strength. The unique microstructure of the alloy, which normally comprises of a cuboid-shaped strengthening γ′ phase homogeneously dispersed in a γ phase matrix, is responsible for the alloy's extraordinary mechanical characteristics. The γ phase is a solid-solution phase with a disordered face-centered cubic (FCC) structure, and the γ′ phase is an intermetallic compound Ni_3Al with an ordered $L1_2$ structure. One of the most effective approaches proven for increasing temperature capability and stabilizing the γ′ phase, as well as achieving magnificent mechanical properties and higher-temperature performance under various service conditions, is to add additional alloying elements to superalloys (Rawlings and Staton-Bevan, 1975; Chiba et al., 1991; Chiba et al., 1992; Gleeson et al., 2004). For instance, Hf, Re, Ta, and W are utilized to enhance mechanical strength and the solvus temperature; B and Zr to enhance ductility; Al, Cr, and Ti improve the corrosion resistance and oxidation (Barrett et al., 1983; Caron and Khan, 1999; Blavette et al., 2007), and the strengthening elements e.g. Nb, Mo, Re, Ta, and W significantly enhanced the mechanical behavior of superalloy (Gariboldi et al., 2008; Wang and Wang, 2009; Amouyal et al., 2010; Bensch et al., 2010). Therefore, the knowledge of the strengthening mechanism of site preferences of alloying elements in the γ′ phase is important for understanding the roles of the substitutional atoms in determining the mechanical properties of Ni-based superalloys.

The site occupying information is indispensable data for a theoretical and quantitative design of alloys. However, it is a long-time challenge for both theoretical and experimental investigations to determine the site preference due to the complex configuration as well as the requirement of the single-crystal sample at the phase equilibrium state. Furthermore, the mechanical properties of Ni_3Al-based γ′ phase alloys are related to the sublattice site occupying behaviors of alloying elements (Chiba et al., 1991). For example, the ductility and ordering energy of Ni_3Al alloys decreases, while its yield strength increases when the Ni site (i.e., 3c sublattice) is substituted by alloying elements. The reliability of γ and γ′ phases was reported by Suzuki (Suzuki and Oya, 1981). If additional elements occupy the 1a sublattice; the γ′-phase will be more stable in the matrix, on the other hand, if elements occupy the 3c sublattice, the γ-phase is more stable, respectively. Therefore, the investigation of the site preference of alloying elements in Ni_3Al is of great practical and fundamental interest. Several attempts have been employed to predict the site occupancy of alloying elements in the γ′ phase. In 1959 s, a phenomenological thermodynamic model was proposed to explain alloying behavior first time, proposing that the electronic structure of the ternary addition determined the site substitution behavior of ternary additions to Ni_3Al (Guard, 1959). Rawlings and Staton-Bevan proposed a strong correlation between the site preferences and mechanical properties of the γ′ phase of the ternary additions (Rawlings and Staton-Bevan, 1975). Hono et al. (Hono et al., 1992) studied the site preferences of Cu and Ge by using atom probe field ion microscopy (APFIM) with different compositions $Ni_{75-x}Al_{23}X_{1-x}$, and their results showed that Cu occupied the 3c sublattice and Ge occupies the 1a sublattice. Geng et al. (Geng et al., 2004) used supercell models based on first-principles total-energy calculations at room temperature to explore the site preference of PGM additions in γ′-Ni_3Al. Their findings demonstrated that Mo favors the 1a sublattice, while Os, Ru, Rh, Pd, Ir, and Pt atoms prefer the 3c sublattice, in which Os shows a weak site preference tendency for the 3c sublattice. Saito and Harada used the Monte Carlo approach to show that Co favors the 3c sublattice in CMSX-4 and TMS63 alloys, whereas Mo, Ta, and Ti favor the 1a sublattice, and Cr occupies both 1a and 3c sublattice. But, there is insufficient experimental data to support their calculation (Saito and Harada, 1997). Jiang et al. (Jiang et al., 2006) predicted the site preference of Pt, Hf, Cr, and Ir in Ni_3Al, as well as the impact of temperature on site preference of ternary alloying elements by utilizing a statistical-mechanical Wagner-Schottky model based on first-principles with different compositions, and calculated the point defect formation enthalpies. By using the atom-probe tomography (APT) and first-principles calculations, Booth and Mao (Booth-Morrison et al., 2008) studied the site preference of Cr and Ta in the Ni_3Al ($L1_2$)-type γ′-precipitates of a ternary system with different compositions, in which Al, Cr, and Ta occupied the 1a sublattice. Kim et al. (Kim et al., 2010) employed the strain–stress method based on first-principles calculations to study the impact of alloying elements (Cr, Hf, Pt, Y, and Zr) on the elastic characteristics and site preference of Ni_3Al alloys at 0 K. Their study revealed that Cr, Hf, Y, and Zr favor the Al sublattice, while Pt prefers the Ni sublattice.

Kumar and Chernatynskiy (Kumar et al., 2015) investigated the influence of alloying elements (Cr, Zr, B, Ce, and La) on the site preferences and the elastic properties of Ni_3Al alloys at room temperature with different compositions. Zhu et al. (Zhu et al., 2020) employed the first density functional theory to elucidate the mechanical properties and site preference of Ni/Ni_3Al alloys doped with Re, Ta, and W at a low temperature of 50 K. Pan et al. employed the first-principles calculations (Chen and Pan, 2022; Pan, 2022; Pan and Chen, 2020; Yu and Pan, 2021; Pan, 2021) to study the site preference, structural stability, electronic, optical, catalytic, thermodynamic, and mechanical properties (Pu and Pan, 2022; Pu and Pan, 2022; Pan and Chen, 2022; Pu and Pan, 2022; Pu and Pan, 2022; Pu and Pan, 2022) of ternary phases as well as high temperature superalloys. According to first-principles calculations (at the ground state) and APT results, Mo and Ti favor the 1a sublattice (Enomoto and Harada, 1989; Mekhrabov et al., 1997; Tu et al., 2012; Raju et al., 1996). The atomic site occupancy of additional elements, including Cr, Co, Re, Ru, Ta, and W, is still elusive based on theoretical predictions (Amouyal et al., 2010; Jiang et al., 2006; Enomoto and Harada, 1989; Mekhrabov et al., 1997; Raju et al., 1996; Wu and Li, 2012; Eriş et al., 2017; Özcan et al., 2009; Amouyal et al., 2014; Amouyal et al., 2009) and experimental data from APT (Amouyal et al., 2010; Saito and Harada, 1997; Booth-Morrison et al., 2008; Tu et al., 2012; Amouyal et al., 2014; Amouyal et al., 2009; Bagot et al., 2017; Blavette and Bostel, 1984; Zhou et al., 2008; Huang et al., 2016), energy dispersive spectroscopy (EDS) (Broderick et al., 2018), and channeling-enhanced microanalysis (Horita et al., 1995; Liebscher et al., 2008).

However, previous theoretical investigations focus only on the site preference at the ground state (0 K) using a supercell model supported with first-principles calculations and calculating the enthalpy of formation of the alloy phase at the ground state. In the previous supercell model, they generally placed the additional alloying element either on the 1a sublattice or on the 3c sublattice, and the corresponding two configurations are $(Ni_{1-x}M_x)_3Al$ and $Ni_3(Al_xM_{1-x})$, respectively. However, the chemical compositions are different for the two configurations, so the site preference of atoms on sublattice judged from the enthalpy of formation of the alloy phase with different compositions may be insufficient. Most importantly, no reasonable theoretical report concerning the effects of heat treatment temperature on the site preference, so it is necessary to thoroughly understand the temperature- and composition-dependent site preference in order to design the Ni-based high-temperature alloys strengthened with γ' phase rationally.

In our prior study, the sublattice model based on the crystal lattice structure information has been widely applied to investigate the temperature-dependent site preference and ordering behaviors concerning $NbCr_2$-based Lave phases with two sublattices (Wu et al., 2013), Ti_2AlNb orthorhombic phase with three sublattices (Wu et al., 2008), $ThMn_{12}$ structure with four sublattices (Zheng et al., 2010), Co-based superalloys (Ali, 2022), as well as in high entropy alloys (Wu et al., 2022), and also employed the first-principle calculations to studied the crystal lattice structure, thermodynamics and mechanical properties in $ZnZrAl_2$ intermetallic compound (Wei et al., 2016); elastic, electronic and thermodynamic properties of the Ti_2AlNb orthorhombic phase (Hu et al., 2017; Wei et al., 2021). In this work, we predicted the temperature- and composition-dependent site occupying preferences of the binary, ternary, and quaternary of Ni_3Al-based γ' phase with an FCC_$L1_2$ structure alloyed with M_i where M_i represents the additional transitional metals Co, Cr, Cu, Fe, Mn, Mo, Re, Ta, Ti, V, and W atoms (arranged in alphabetical order), were studied using a two-sublattice thermodynamic model $(Ni, Al, M_i)_{1a}(Ni, Al, M_i)_{3c}$. The site occupying fractions (SOFs) were calculated using a thermodynamic software package based on a thermodynamic database established in this work, where the temperature-dependent thermodynamic data were obtained using first-principles calculations based on density-functional theory (DFT) and density-functional perturbation theory (DFPT). Based on calculated SOFs results, we studied the mechanical and thermodynamic properties at the ground state (0 K), which agree well with both theoretical and experimental data in the available literature. Our approach is general for any given composition of Ni_3Al-based γ' phase with an FCC_$L1_2$ structure alloyed with one or more additional transitional metal M_i. For this purpose, we presented the model computation methodology, and the results of some selective Ni_3Al-based γ' phases with an FCC_$L1_2$ structure alloyed with M_i.

2. Theoretical methodology and computational approaches

2.1. Sublattice model

The prototype of the Ni_3Al-based γ' phase with an FCC_$L1_2$ structure is the full ordered $AuCu_3$. The crystallographic information is shown in Table 1. The combination of multiplicity and Wyckoff letter of Wyckoff positions are generally named as 1a sublattice and 3c sublattice, thus the Au atoms are localized at the cube corner (1a sublattice) and the Cu atoms are localized at the face centers (3c sublattice).

In this work, we do not premeditate the site preferences and suppose that each type of alloying element including Ni, Al, and M atoms, can occupy both sublattice 1a and 3c with a probability, i.e., the SOFs. So, the configuration of the FCC_$L1_2$ γ'-Ni_3Al phase alloying with additional transition metals M can be described with the following general two-sublattice model in **Eq. (1)**,

$$\left(Al_{y_{Al}^{1a}}, Ni_{y_{Ni}^{1a}}, M1_{y_{M1}^{1a}}, M2_{y_{M2}^{1a}}, \cdots, Mi_{y_{Mi}^{1a}}\right)_{1a}\left(Al_{y_{Al}^{3c}}, Ni_{y_{Ni}^{3c}}, M1_{y_{M1}^{3c}}, M2_{y_{M2}^{3c}}, \cdots, Mi_{y_{Mi}^{3c}}\right)_{3c} \quad (1)$$

where 1*a* and 3*c* are the Wyckoff notation of the sublattice as mentioned above, y_{Mi}^{1a} and y_{Mi}^{3c} are the site fraction of element '*i*' (including Al, Ni, and any other additional alloying elements) on sublattice 1*a* and 3*c*. The thermodynamic principles of phase equilibrium may be used to determine the SOFs for a particular alloy composition at equilibrium heat treatment temperature. To quantitatively describe the alloy's thermodynamics, we consider the formation of the alloy phase to a general chemical reaction from pure elements to the complex γ' phase. For example, for the system of a total of 100 atoms including 72Ni, 24Al, and 4M atoms, the chemical reaction process of the formation of the γ'-$Ni_3(Al, M)$ phase with FCC_$L1_2$ structure created from the respective pure elements is given in **Eq. (2)**,

Table 1 The crystallographic information of the FCC_$L1_2$ phase with the full ordered $AuCu_3$ as a prototype.

Prototype	Pearson's Symbol	Strukturbericht Designation	Space group		Wyckoff positions		
			Symbol	Number	Atom	Multiplicity	Wyckoff letter
$AuCu_3$	cP4	$L1_2$	Pm3m	221	Au	1	a
					Cu	3	c

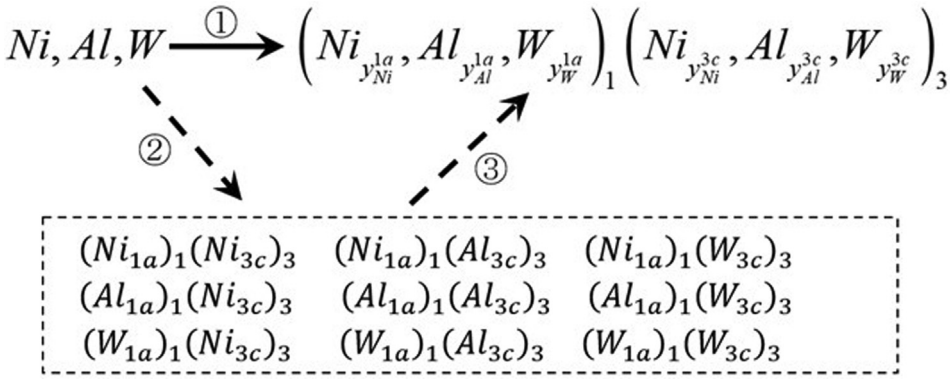

Fig. 1 The alternative computation path of the thermodynamic function, i.e., ①=②+③.

$$72Ni + 24Al - 4M = 25[y_{Ni}^{1a}(Ni) + y_{Al}^{1a}(Al) + y_{M}^{1a}(M)] + 75[y_{Ni}^{3c}(Ni) + y_{Al}^{3c}(Al) + y_{M}^{3c}(M)] \quad (2)$$

where there are 100 total atom sites, including 25 sites belonging to sublattice 1a, and 75 sites belonging to sublattice 3c. For a particular alloy composition and temperature, the unknowns are a series of SOFs, and unknowns can be analytically solved using some fundamental physical and chemical principles supported by several professional software packages such as Vienna Ab initio Simulation Package (VASP), PHONOPY, Thermo-Calc and PANDAT (Kresse and Furthmüller, 1996; Baroni et al., 2001; Andersson et al., 2002; Chen et al., 2002), which will be described concisely later. Once the SOFs at various temperatures and compositions are obtained, thus the order–disorder transformation may be studied comprehensively (Wu et al., 2008). Based on the properties of the thermodynamic function whose quantity is distinctively defined by the initial and final states, and is independent of the intermediate process, we adopted a different framework to compute the Gibbs energy of the formation of the γ′–Ni_3Al-based intermetallics with FCC_$L1_2$ structure constituted from the stable pure elements at room temperature, here we take the γ′–Ni_3Al alloyed by additional W atoms as an example, is shown in Fig. 1.

Firstly, the hypothetical end-members (i.e., compounds with sublattices fully occupied by only one type of atom) are created from pure elements, and secondly, the γ′ phase formed from the end-members, i.e., ①=②+③. For example, the Gibbs energy of formation of the single-phase FCC_$L1_2$ γ′ phase derived from the pure elements can be calculated by **Eq. (3)**,

$$\Delta G = \sum_{i=1}^{n}\sum_{j=1}^{n} y_{M_i}^{1a} y_{M_j}^{3c} \Delta G_{(M_i^{1a}:M_j^{3c})} - T\left(-R\sum_{i=1}^{n}\sum_{j=1}^{n}(y_{M_i}^{1a}.lny_{M_i}^{1a} + y_{M_i}^{3c}\hat{\mathrm{A}}\cdot lny_{M_i}^{3c})\right) \quad (3)$$

where $\Delta G_{(M_i^{1a}:M_j^{3c})}$ represents the Gibbs free energy of formation of the end-members $(M_i)_{1a}(M_j)_{3c}$ is constituted from the pure elements with a stable structure at room temperature, i.e., the so-called stable element reference state (SER). $\Delta G_{(M_i^{1a}:M_j^{3c})}$ is the essential thermodynamic data to elucidate the thermodynamic approach, which was calculated and depicted as a structured thermodynamic database file (Gamma-prime-end-member. TDB) and $y_{M_i}^{S_k}$ is the SOF of each type of atom on each type of sublattice, where the unit of G and ΔG were normalized to J/(mol·atom). We calculated the thermodynamic characteristics at a certain temperature using the quasi-harmonic approximation (QHA), which involves vibrational and electronic impacts. The thermal excitation of the electron was not taken into account in this study, but it is important to consider it further by integrating the ab initio calculation with calorimetric observations. When the heat treatment of the Ni_3Al-based γ′ alloy phase achieves its equilibrium state, the Gibbs energy of formation of the alloy, ΔG, must present a minimum, which is given in **Eq. (4)**,

$$\frac{\partial(\Delta G)}{\partial(y_{M_i}^{S_k})} = 0 \quad (4)$$

We got **Eq. (5)** and **Eq. (6)** by assuming mass balance and composition normalization as:

$$\sum_{i=1}^{n} y_{M_i}^{S_k} = 1 \quad (5)$$

$$\sum_{k=1}^{n} f_{S_k} * y_{M_i}^{S_k} = x_{M_i} \quad (6)$$

Once the value of $\Delta G_{(M_i^{S_k}:M_j^{S_l})}$ at definite temperature is obtained, the relationship of SOFs with temperature and composition can be determined as seen from **Eq. (7)**,

$$y_{M_i}^{S_k} = f(x_{M_i}, T) \quad (7)$$

Thus, the site preference and thermodynamic functions of the Ni_3Al-based γ′ alloy phase were easily estimated based on the predicted temperature and composition-dependent site occupying fractions.

2.2. Thermodynamic database of Gibbs free energy of formation of end-members

The Gibbs free energies of formation $\Delta G_{(M_i^{S_k}:M_j^{S_l})}$ of the end-members may be determined using **Eq. (8)**,

$$\Delta G_{(M_i^{S_k}:M_j^{S_l})} = G_{(M_i^{S_k}:M_j^{S_l})} - f_{S_k} * G_{(M_i)} - f_{S_l} * G_{(M_j)} \quad (8)$$

where $G_{(M_i^{S_k}:M_j^{S_l})}$ and $G_{(M_i)}$ are the temperature-dependent Gibbs free energy function of all the end-member compounds

and pure elements with SER, f_{S_k} and f_{S_l} are the fraction of a different kind of sublattice. The QHA approach (Togo et al., 2008) was used to determine the Gibbs free energy of each end-member and pure element as SER at finite temperature, and the temperature-dependent Gibbs free energies of end-members and the corresponding pure elements with SER were calculated by employing the linear response method i.e., DFPT at an external pressure of 1 atm. At the ground state, the first-principles calculations were based on the DFT (Jain et al., 2016; Lejaeghere et al., 2016) within the generalized gradient approximations (GGA) by VASP (Thygesen and Jacobsen, 2016) with the ion–electron interaction expressed by the projector augmented wave (PAW) approach (Blöchl, 1994; Kresse and Joubert, 1999) and the exchange–correlation functional defined by the GGA of Perdew-Burke-Ernzerhof (PBE) (Perdew et al., 1996). Considering the available computing resource, the calculation of the mechanical properties uses a $3 \times 3 \times 3$ supercell based on the FCC_$L1_2$ $AuCu_3$ prototype, with a total of 108 atoms involved in the calculations. We set ISPIN = 2 to perform spin-polarized calculations, and the cutoff kinetic energy of 500 eV was used. The Gibbs free energy and phonon frequencies were computed from the force constants utilizing the Phonopy tool in combination with the QHA model and VASP, and DFPT (Baroni et al., 2001; Baroni et al., 2010) was utilized to compute the force constants. The Brillouin zone sampling is implemented by the Monkhorst–Pack scheme (Monkhorst and Pack, 1976) with (KPOINTS) was set as $6 \times 6 \times 6$ Monkhorst-Pack mesh for AB_3_$L1_2$ (ordered FCC, 4 atoms in the primitive cell) end-members. All of the calculation parameters revealed that the overall energy convergence threshold was less than 2 meV/atom at 0 K. **Table S1** summarizes the Brillouin zone sampling (KPOINTS) and supercell dimension of several types of end-members and pure elements involved in this research work. The expression of free energy and temperature in this work is given in **Eq. (9)** (Abe et al., 2006);

$$G(T) = A + BTlnT + CT^2 + DT^3 + ET^{-1} + FT \tag{9}$$

where $G(T)$ denotes the Gibbs free energy of pure elements and end-member compounds as a function of temperature, and T is the temperature (Kelvin), A, B, C, D, E, and F are the different coefficients. After that, we developed a formatted thermodynamic database of Gibbs free energies of formation of end-member compounds employed in this research work, which was used by the thermodynamics software package PANDAT or Thermo-Calc to calculate thermodynamic functions and fine phase structures under phase equilibrium. Thus, we acquired a thorough understanding of how distinct thermodynamic functions and SOFs varied with different alloy compositions and heat treatment temperatures, respectively.

2.3. Elastic constants

The stress–strain method (Shang et al., 2007) is used to calculate the elastic constants (C_{ij}). During ionic position relaxations, the volume and cell (Pu and Pan, 2022) structure are fixed, and only the forces acting on ions can be relaxed. The elastic constants in terms of Hook's law are expressed as,

$$\sigma i = \sum_{j=1}^{6} C_{ij}.\varepsilon i = \begin{pmatrix} \sigma_1 \\ \sigma_2 \\ \sigma_3 \\ \sigma_4 \\ \sigma_5 \\ \sigma_6 \end{pmatrix} = \begin{pmatrix} C_{11} & C_{12} & C_{13} & C_{14} & C_{15} & C_{16} \\ C_{21} & C_{22} & C_{23} & C_{24} & C_{25} & C_{26} \\ C_{31} & C_{32} & C_{33} & C_{34} & C_{35} & C_{36} \\ C_{41} & C_{42} & C_{43} & C_{44} & C_{45} & C_{46} \\ C_{51} & C_{52} & C_{53} & C_{54} & C_{55} & C_{56} \\ C_{61} & C_{62} & C_{63} & C_{64} & C_{65} & C_{66} \end{pmatrix} \times \begin{pmatrix} \varepsilon_1 \\ \varepsilon_2 \\ \varepsilon_3 \\ \varepsilon_4 \\ \varepsilon_5 \\ \varepsilon_6 \end{pmatrix} \tag{10}$$

where σ_i and ε_i are stress and strain vectors respectively. There are six independent components of strain $\varepsilon = (\varepsilon_1, \varepsilon_2, \varepsilon_3, \varepsilon_4, \varepsilon_5, \varepsilon_6)$ where ε_1, ε_2, ε_3 indicate the normal strains and ε_4, ε_5, ε_6 indicate the shear strains, are performed on a crystal to formulate the small deformation, and the given set of stress $\sigma = (\sigma_1, \sigma_2, \sigma_3, \sigma_4, \sigma_5, \sigma_6)$ can be described on the deformed lattice with the assistance of first-principles calculations. The change in the total energy of the system after applying strain to the material can be expressed by the Taylor series (Fast et al., 1995);

$$\Delta E(V, \{\varepsilon_i\}) = E(V, \{\varepsilon_i\}) - E(V_0 - 0) = \frac{Vo}{2} \sum_{i,j=1}^{6} C_{ij}.\varepsilon i \varepsilon j \tag{11}$$

where ΔE is the change value of total energy before and after applying strain, and V_0 is the equilibrium volume without applying strain. There are three independent elastic constants for an $L1_2$-type cubic structure: C_{11}, C_{12}, and C_{44}, which may be computed as,

$$\sigma = \begin{bmatrix} C_{11} & C_{12} & C_{12} & 0 & 0 & 0 \\ C_{12} & C_{11} & C_{12} & 0 & 0 & 0 \\ C_{12} & C_{12} & C_{11} & 0 & 0 & 0 \\ 0 & 0 & 0 & C_{44} & 0 & 0 \\ 0 & 0 & 0 & 0 & C_{44} & 0 \\ 0 & 0 & 0 & 0 & 0 & C_{44} \end{bmatrix} \tag{12}$$

Then we used Voigt-Reuss-Hill (VRH) approximation (Ledbetter and Reed, 1973; Xiong and Gu, 2015) to calculate the polycrystal elastic moduli i.e., bilk (B), shear (G), and Young's (E) modulus and Poisson ratio (ν), respectively.

3. Results and discussions

3.1. The Gibbs free energy of pure elements at SER and end-members

In this work, there are 13 alloying elements involved, including Al, Co, Cr, Cu, Fe, Mn, Mo, Ni, Re, Ta, Ti, V, and W, thus 169 (13×13) end-members with FCC_$L1_2$ structure were created. The essential details of the pure element of their stable structure at room temperature employed in this work are summarized in **Table S2**. The calculated scattered data of Gibbs free energies using the QHA model of all the pure elements at SER and end-members involved in this work were plotted and then fitted using **Eq. (9)**. Both the calculated scattered data of Gibbs free energies and the fitted curve for the representative pure element Ni_FCC were plotted in **Fig. S1**, and those for the representative end-member $(Al)_{1a}$ $(Ni)_{3c}$ with a full ordered structure were plotted in **Fig. S2**, while the scattered data of the rest pure elements with SER structure were plotted in **Fig. S3**, the scattered data of the rest end-members were

plotted in Fig. S4. It can be observed that the fitted curve covers the scattered data quite well, all the plots show very smooth, and the fitted deviations are considerably small. To further validate the computation's accuracy and validity, the bulk moduli and lattice constants of pure elements at 0 K derived via phonon calculation are listed in Table S3, which accord very well with the currently available literature. The fitting formula of the temperature-dependent Gibbs free energy of pure element Ni_FCC, and end-member $(Al)_{1a}(Ni)_{3c}$ are given in **Eq. (13)** and **Eq. (14)**,

$$\begin{aligned} G(\text{Ni\_FCC}) = & -5.34E+05-18.04*T*LN(T) \\ & -0.008461*T**2+11.45E-07*T \\ & **3-2.43E+04*T**(-1)+84.31*T \end{aligned} \tag{13}$$

$$\begin{aligned} G(\text{FCC, AL : Ni}) = & -5.32E+05-12.94*T*LN(T) \\ & -0.001217*T**2+14.19E-07*T \\ & **3+2.352E+04*T**(-1)+65.38 \\ & *T-0.25*\text{SERAL\#}-0.75\text{SERNi\#} \end{aligned} \tag{14}$$

where SERAL# and SERNi# are the temperature-dependent Gibbs free energies of the pure elements Al and Ni with their stable structures at room temperature, respectively, i.e., the so-called stable element reference state (SER) mentioned in Section 2.2. The enthalpy of formation of end-member at the ground state $\Delta H_{\left(M_i{}^{S_k}:M_j{}^{S_l}\right)}$ is an essential thermodynamic function, that can be used to estimate the feasibility of the synthesis, which is derived from the first-principles total-energy calculations using **Eq. (15)**,

$$\Delta H_{\left(M_i{}^{S_k}:M_j{}^{S_l}\right)} = E_{tot\left(M_i{}^{S_k}:M_j{}^{S_l}\right)} - f_{S_k} * E_{tot\left(M_i{}^{S_k}\right)} - f_{S_l} * E_{tot\left(M_i{}^{S_l}\right)} \tag{15}$$

where $E_{tot\left(M_i{}^{S_k}:M_j{}^{S_l}\right)}$ is the total energy of the end-member, $E_{tot\left(M_i{}^{S_k}\right)}$ and $E_{tot\left(M_j{}^{S_l}\right)}$ are the total energy of the corresponding elements, respectively. Normally, if the heat output is negative, it means that the synthesis reaction can happen spontaneously. As previously stated, all thermodynamic functions ΔG, and ΔH are normalized to J/(mol·atom). The calculated E_{tot} for all pure elements were presented in Table S4, while the E_{tot}, enthalpy of formation ΔH_f (at 0 K) based on **Eq. (15)**, and the Gibbs free energies of formation ΔG based on **Eq. (8)** at temperatures 300 K and 1000 K for all end-

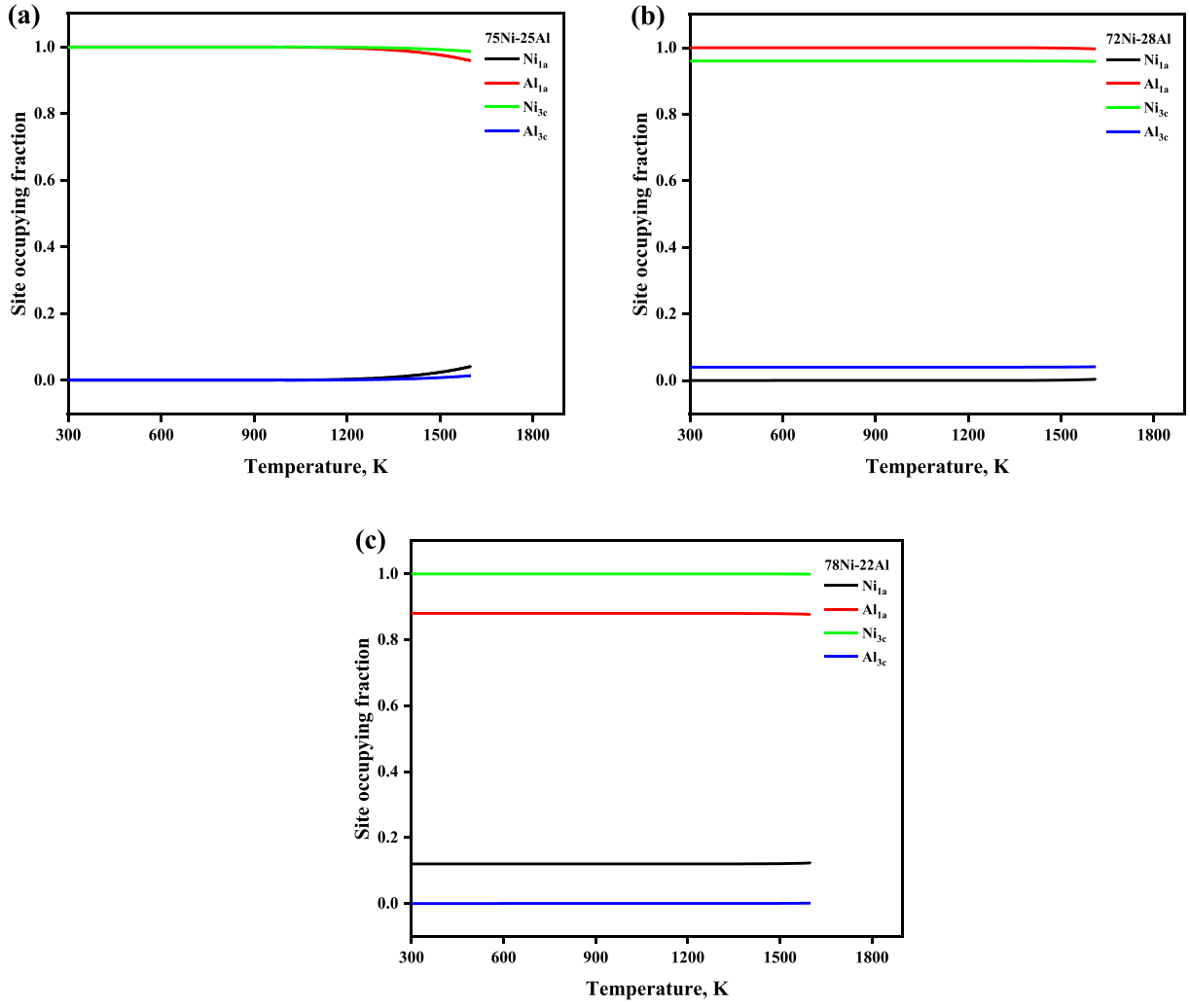

Fig. 2 The temperature-dependent site occupying fraction of stoichiometric and nonstoichiometric Ni_3Al-based γ' phase.

members $(Al)_{1a}(B)_{3c}$ involved in this study are tabulated in Table S5, and the rich fundamental genome data are essential for Ni-based superalloys design.

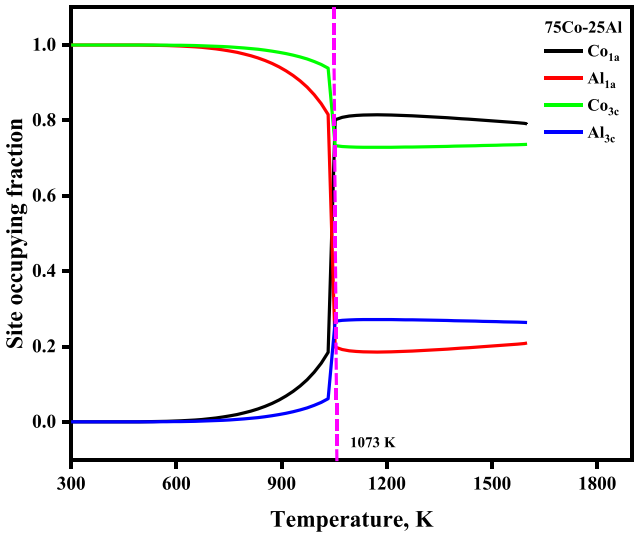

Fig. 3 The temperature-dependent site occupying fraction of stoichiometric Co_3Al-based γ' phase.

3.2. Temperature-dependent site preference and thermodynamic functions

The temperature-dependent SOFs and thermodynamics functions of the Ni_3Al-based γ' phase were calculated and plotted in Fig. 2 to Fig. 8, where the thermodynamic functions include Gibbs free energy of formation, enthalpy of formation, the entropy of formation, as well as configurational entropies. The temperature-dependent SOFs of stoichiometric and non-stoichiometric Ni_3Al-based binary γ' phases are presented in Fig. 2. From Fig. 2**(a),** It has been observed that the Ni_3Al-based γ' phase shows full order behavior in the whole temperature range, and its site configuration changes from $(Al)_{1a}(Ni)_{3c}$ at room temperature to $(Al_{0.9984}Ni_{0.0015})_{1a}(Al_0Ni_{0.9994})_{3c}$ at 1273 K, where Al atoms favor sublattice 1a and Ni atoms favor 3c sublattice. Moreover, we have observed that the site preferences of Ni atoms are slightly affected by the heat treatment, for example, at low temperature i.e., 298 K, Ni atoms occupy the 3c sublattice exclusively, but when the heat treatment is higher than 1273 K, then Ni atoms occupied both the sublattices but preferred to 3c, whereas Al atoms always occupied 1a sublattice in the whole temperature range. Furthermore, to deeply understand and verify this, we also plotted the SOFs of the nonstoichiometric Ni_3Al-based γ' phase. From Fig. 2**(b)** and Fig. 2**(c)**, we found that the nonstoichiometric

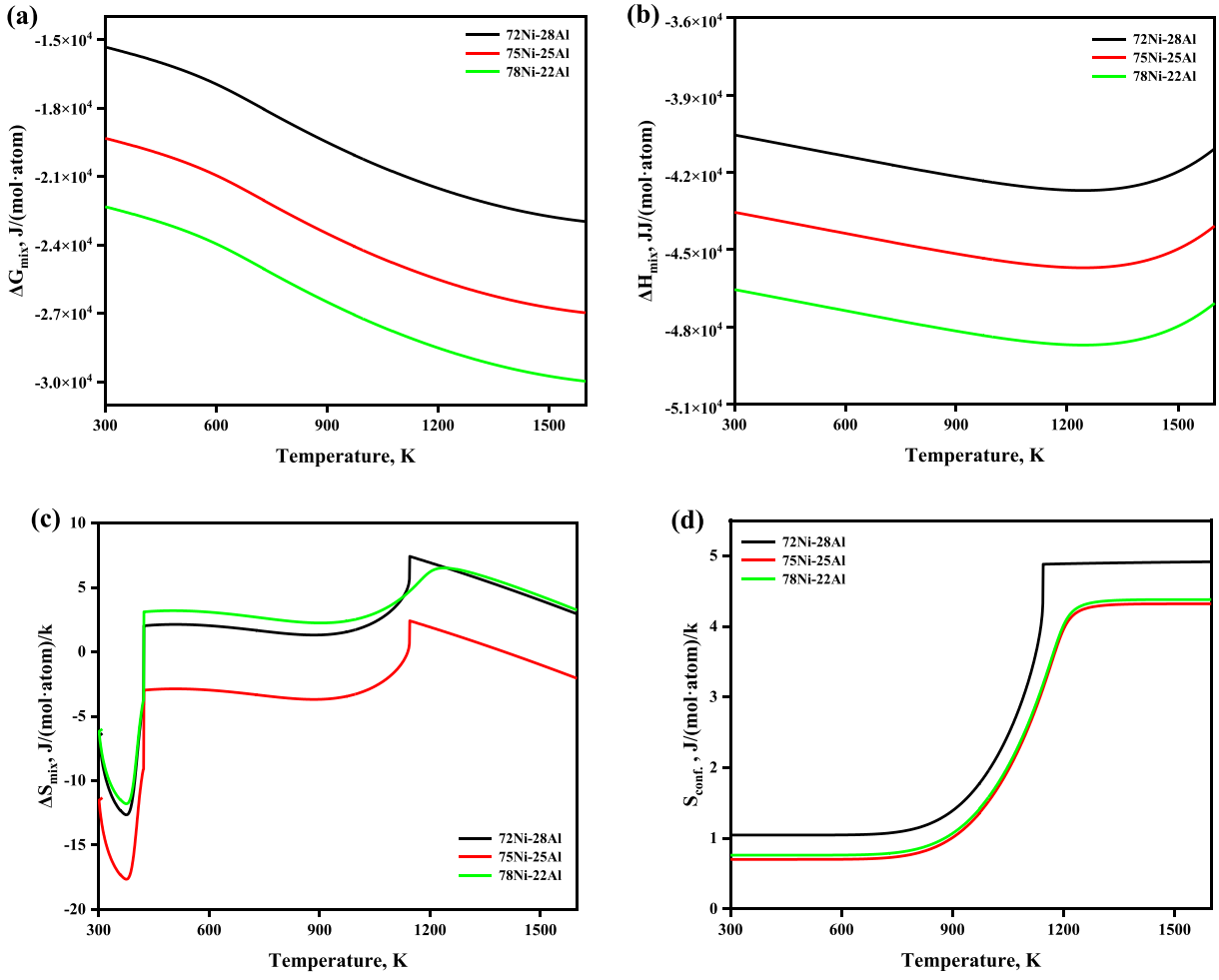

Fig. 4 The temperature-dependent thermodynamic functions of stoichiometric and nonstoichiometric Ni_3Al-based γ' phase.

case also shows the similar behavior which was observed in the stoichiometric case. At low temperature i.e., 298 K, Ni atoms occupy 3c sublattice exclusively, but when the heat treatment is higher than 1273 K, then Ni atoms occupied both the sublattices but preferred to 3c, whereas Al atoms always occupied 1a sublattice in the whole heat treatment process. As a counterpart of the Ni_3Al-based γ' phase, we also investigated the site preference of the stoichiometric Co_3Al-based γ' phase,

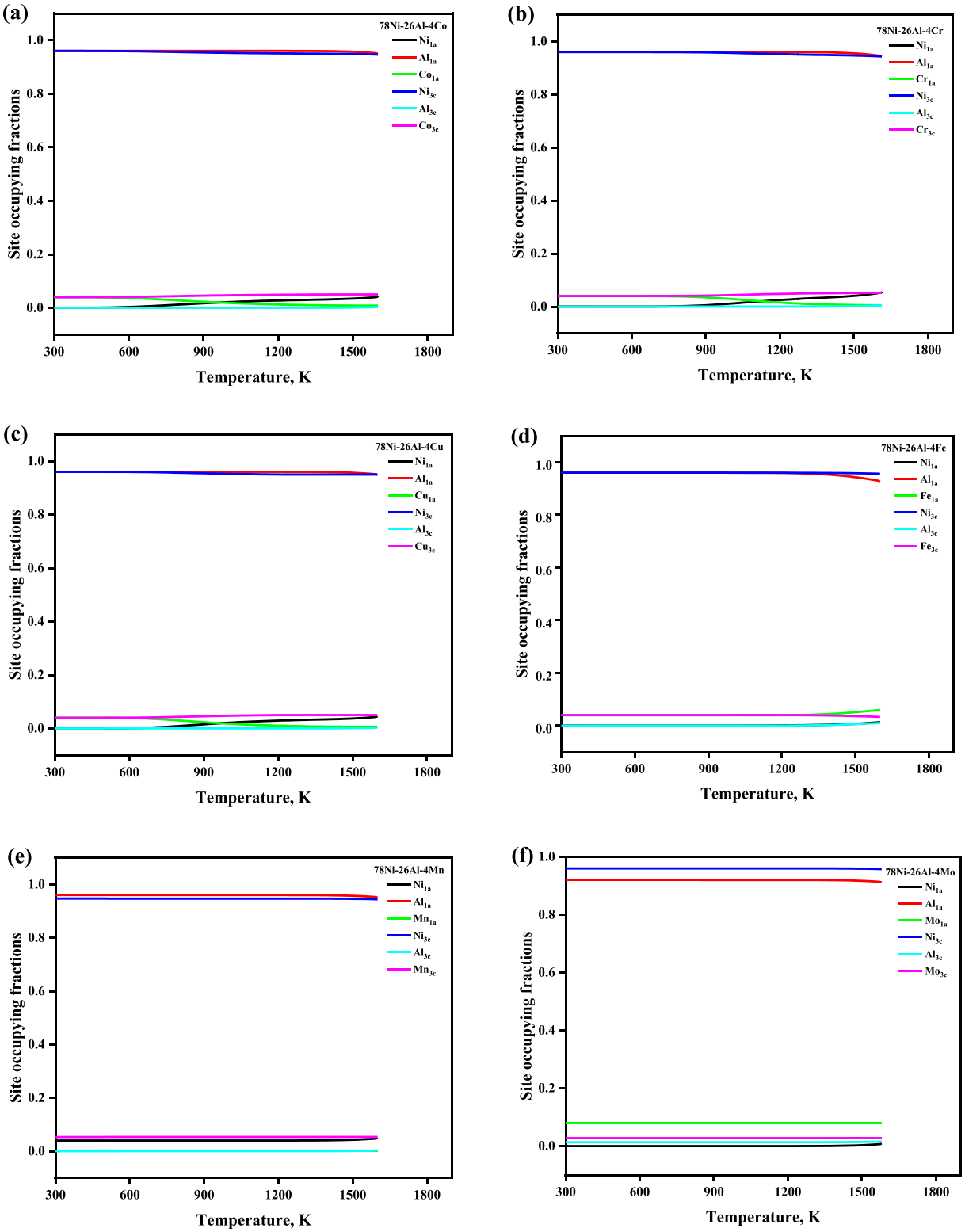

Fig. 5 The temperature- and composition-dependent SOFs of the alloying element in Ni_3Al-based γ' phase with the composition 78Ni-26Al-4M_i, which is normalized as 72.22Ni-24.08Al-3.7M_i (at. %).

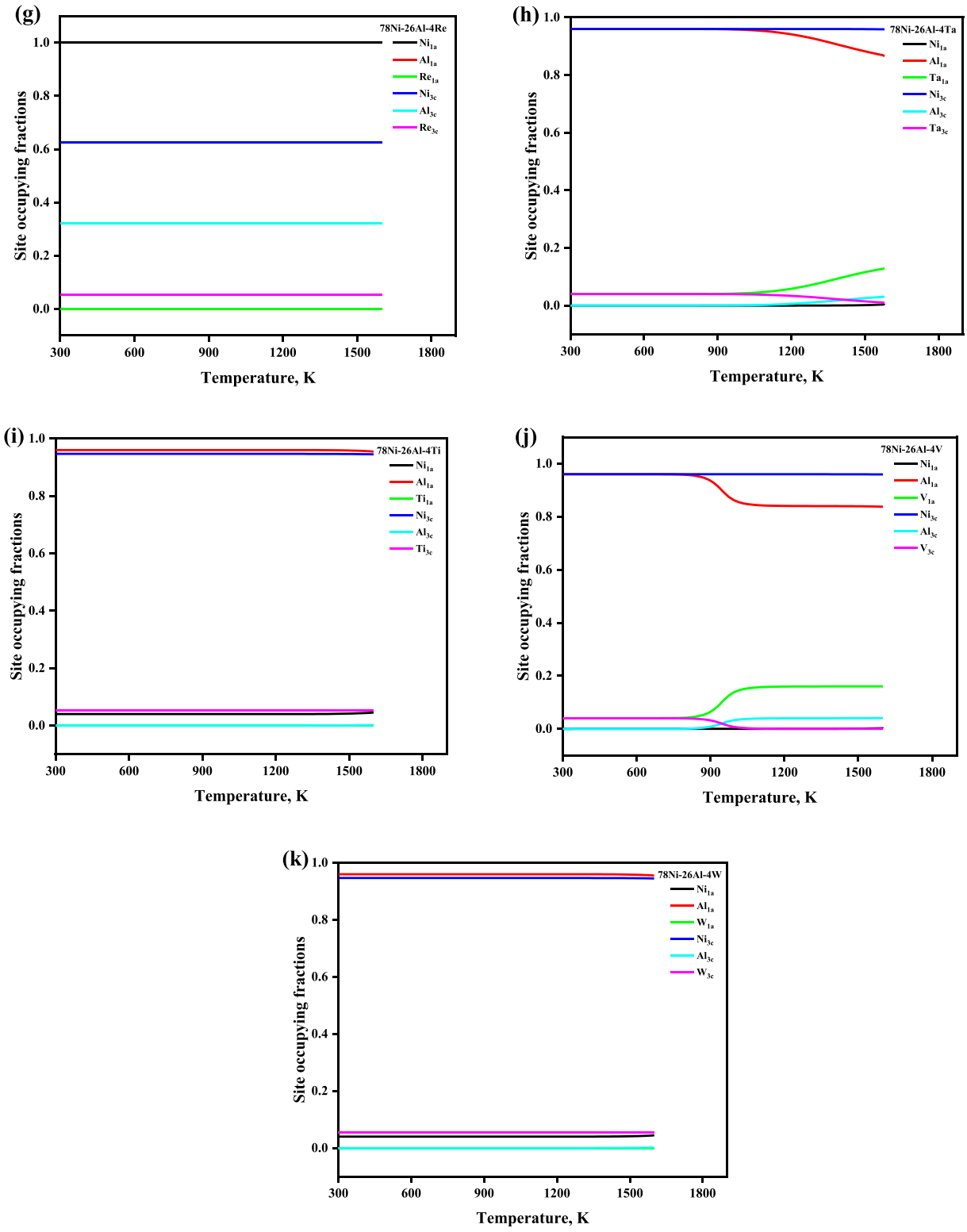

Fig. 5 (*continued*)

illustrated in Fig. 3. From Fig. 3, it is seen that there is a strong order–disorder transition for the stoichiometric Co_3Al-based binary γ' phase, the critical temperature of the order–disorder transition is about 1073 K, accompanied by the site configuration changes from $(Al)_{1a}(Co)_{3c}$ at room temperature to $(Al_{0.2590}Co_{0.7409})_{1a}$ $(Al_{0.2469}Co_{0.7530})_{3c}$ at 1273 K, where Al atoms occupy 1a sublattice exclusively, and Co atoms occupy 3c sublattice exclusively.

The temperature-dependent thermodynamic functions of stoichiometric and nonstoichiometric Ni_3Al intermetallic are

illustrated in Fig. 4 to explore the thermodynamic mechanism of the ordering behavior of the Ni_3Al-based binary γ′ phase. It is noted that ΔG_{mix} decreases as temperature increases; the lower the Gibbs energy, the more stable the structure (Wu et al., 2008), and the rest of the thermodynamic functions changes with the temperature considerably, where the plots of configurational entropies were further calculated using **Eq. (16)** based on the SOFs obtained in this work.

$$S_{Conf.} = -R \times \left(0.25 \times \sum_{i=1}^{n} y_{M_i}^{1a} \times lny_{M_i}^{1a} + 0.75 \times \sum_{i=1}^{n} y_{M_i}^{3c} \times lny_{M_i}^{3c} \right) \quad (16)$$

where R is the gas constant, n is the type number of the constituent atoms.

Following the understanding of the ordering behavior of the Ni_3Al-based binary γ′ phase, we explored the ordering behaviors of the additional alloying element M_i on the Ni_3Al-based γ′ phase further, where eleven additional transition metals M_i, including Co, Cr, Cu, Fe, Mn, Mo, Re, Ta, Ti, V, and W (arranged in alphabetical order) were investigated, which are the commonly used elements in Ni-based superalloy. The sublattice model proposed in this work can be used to predict the SOFs of Ni_3Al-based γ′ phase with any composition, however, for simplifying the question to understand the site preference of additional alloying elements, here we fixed the x_{Ni}/x_{Al} at 3:1 and set the demonstrated composition as composition 78Ni-26Al-4M_i, which is normalized as 72.22Ni-24.08Al-3.7M_i (at. %). Notice that the reason for the composition choice will be mentioned again later, i.e., to agree with the total atom number 108 for a 3 × 3 × 3 supercell of the AB_3_$L1_2$ structure. The temperature-dependent SOFs of the alloying element in the Ni_3Al-based γ′ phase with the composition 78Ni-26Al-4M_i are shown in Fig. 5, and the corresponding temperature- and composition-dependent thermodynamic functions were plotted together in Fig. 6, and we have observed that ΔG_{mix}, ΔH_{mix}, and ΔS_{mix} are decreasing with the increase of the heat treatment, and configurational entropy S_{conf} is increasing with the increase of the temperature, which shows that the doping of ternary elements enhances the structural stability, respectively. As seen in Fig. 5, the atoms are not randomly distributed on the lattice but have a specific site preference. Co, Mn, and Ti atoms always prefer 3c sublattice (Ni site), and Mo atoms always occupied both the sublattice, but preferred the 1a sublattice (Al site) in the whole temperature range, while the site preference of the alloying elements such as Cr, Cu, Fe, Re, Ta, V, and W atoms is affected by the heat

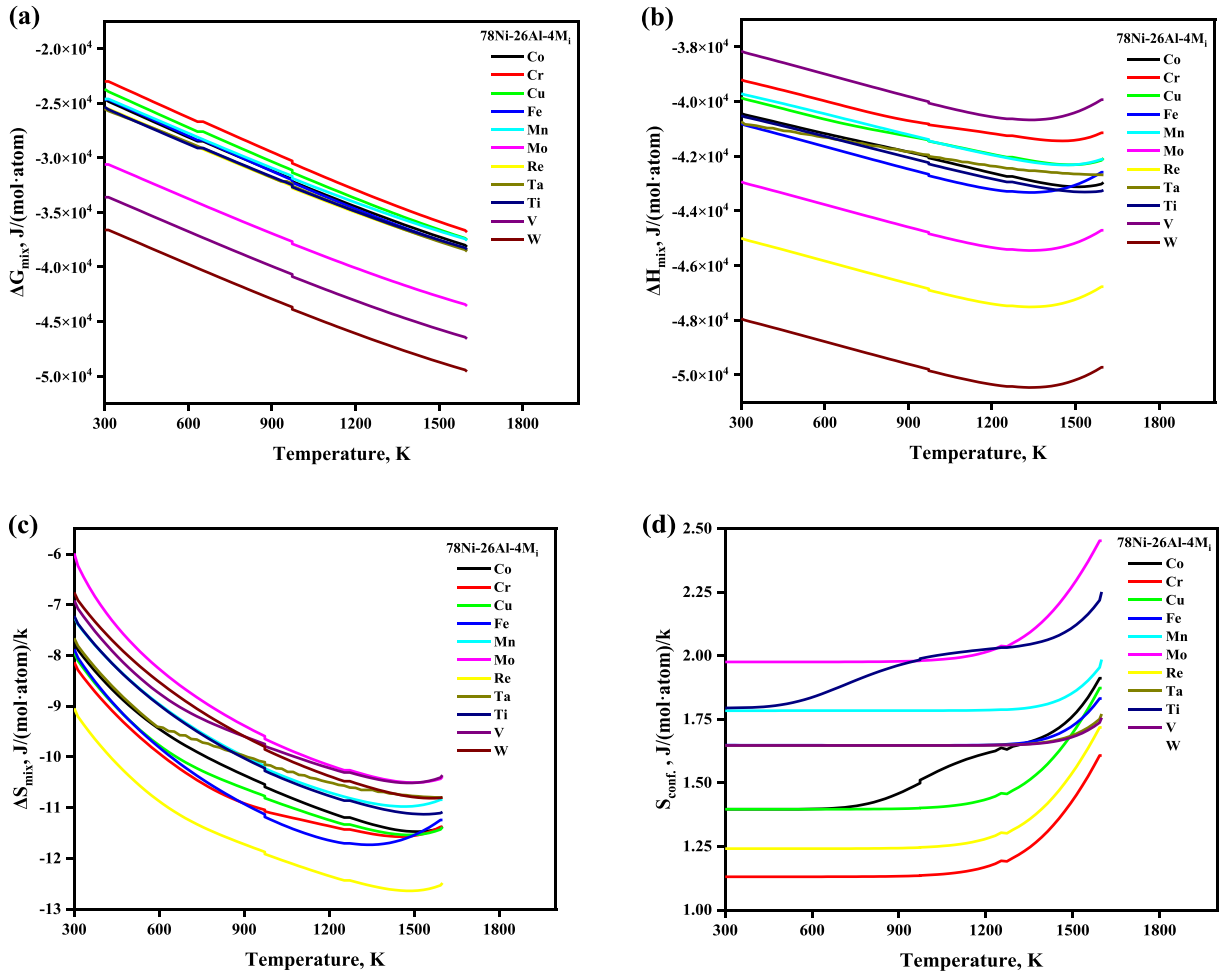

Fig. 6 The temperature- and composition-dependent thermodynamic functions of the alloying element in Ni_3Al-based γ′ phase with the composition 78Ni-26Al-4M_i, which is normalized as 72.22Ni-24.08Al-3.7M_i (at. %).

treatment temperature. For instance, when the heat treatment temperature is lower than 700 K, Cr, Cu, Fe, Ta, V, and W atoms occupy the 1a and 3c sublattice randomly, and Re atoms prefer to 3c sublattice, while when the heat treatment temperature is higher than 1273 K, Cr, Cu, and W atoms prefer 3c sublattice, Fe, Ta atoms prefer to 1a sublattice, while all Re atoms occupy 3c sublattice exclusively, and all V atoms occupy 1a sublattice exclusively, respectively. Our calculated SOFs results (at the ground state) are highly consistent with the theoretical and experimental results in the available literature, except for Ti atoms, which were reported to occupy 1a sublattice at the ground state (Jinlong et al., 1993; Sluiter and Kawazoe, 1995; Ding et al., 2020). The calculated site preferences of alloying elements in the ternary Ni_3Al-based γ' phase compared with the available literature were tabulated in Table 2.

The site preference of the quaternary system with a selective composition 78Ni-26Al-2 M_1-2 M_2, which is normalized as 72.22Ni-24.08Al-1.85 M_1-1.85 M_2 (at. %) was also investigated, and the SOFs were plotted in Fig. 7. It is revealed that Co, Cu, Mn, Re, Ta, V, and W atoms prefer 3c sublattice (Ni site), Ti prefers 1a sublattice (Al site), in the whole temperature

Table 2 Calculated site preferences of alloying elements in ternary Ni_3Al-based γ' phase compared with the available literature.

Ternary elements	Site preference			Ref.
	This work		Other work	
	at ground state	at 1273 K	at ground state	
Co	3c	both	1a	Calc. (Eriş et al., 2021)
			3c	Calc. (Saito and Harada, 1997; Jinlong et al., 1993; Sluiter and Kawazoe, 1995; Ruban and Skriver, 1997; Song et al., 2001)
				Expt. (Ding et al., 2020)
			both	Calc. (Eriş et al., 2021)
				Expt. (Liu et al., 2016)
Cr	both	3c	N	Calc. (Raju et al., 1996; Sluiter and Kawazoe, 1995)
			1a	Calc. (Jiang et al., 2006; Kim et al., 2010; Kumar et al., 2015; Zhu et al., 2020; Eriş et al., 2021; Song et al., 2001; Kim et al., 2012; Chaudhari et al., 2012)
				Expt. (Booth-Morrison et al., 2008; Ding et al., 2020; Liu et al., 2016; Chaudhari et al., 2013; Miller et al., 1994; Shindo et al., 1988)
			3c	Calc. (Cui et al., 2012; Murakami et al., 1994)
				Expt. (More and Miller, 1988)
			both	Calc. (Saito and Harada, 1997; Song et al., 2001)
				Expt. (Kovarik et al., 2009)
Cu	both	3c	3c	Calc. (Jinlong et al., 1993; Sluiter and Kawazoe, 1995)
				Expt. (Hono et al., 1992)
			both	Calc. (Eriş et al., 2021)
Fe	both	1a	N	Calc. (Jinlong et al., 1993)
			3c	Calc. (Sluiter and Kawazoe, 1995; Ruban and Skriver, 1997; Song et al., 2001)
			both	Calc. (Eriş et al., 2021)
Mn	both	3c	3c	Calc. (Sluiter and Kawazoe, 1995)
				Expt. (Wojnecki et al., 2004)
			both	Calc. (Eriş et al., 2021; Song et al., 2001)
Mo	both	1a	1a	Calc. (Geng et al., 2004; Jinlong et al., 1993; Sluiter and Kawazoe, 1995; Eriş et al., 2021; Zhao et al., 2015)
				Expt. (Ding et al., 2020; Yu et al., 2008)
			both	Calc. (Song et al., 2001)
Re	3c	3c	1a	Calc. (Zhu et al., 2020; Eriş et al., 2021; Zhao et al., 2015; Gong et al., 2018)
				Expt. (Ding et al., 2020; Murakami et al., 1994; Umićević et al., 2016)
			3c	Calc. (Raju et al., 1996; Zhou et al., 2008; Cui et al., 2012; Wang et al., 2001)
				Expt. (Cui et al., 2012)
Ta	both	1a	1a	Calc. (Saito and Harada, 1997; Zhu et al., 2020; Sluiter and Kawazoe, 1995; Zhao et al., 2015)
				Expt. (Booth-Morrison et al., 2008; Ding et al., 2020; Garimella et al., 2008)
Ti	3c	3c	1a	Calc. (Saito and Harada, 1997; Jinlong et al., 1993; Sluiter and Kawazoe, 1995)
				Expt. (Ding et al., 2020)
V	both	1a	1a	Calc. (Jinlong et al., 1993; Sluiter and Kawazoe, 1995; Brooks, 1988)
W	both	3c	1a	Calc. (Zhu et al., 2020; Sluiter and Kawazoe, 1995; Eriş et al., 2021; Song et al., 2001; Kovarik et al., 2009; Gong et al., 2018; Chen et al., 2019)
				Expt. (Ding et al., 2020; Murakami et al., 1994; More and Miller, 1988; Umićević et al., 2016)
			3c	Calc. (Cui et al., 2012)
			both	Calc. (Song et al., 2001)

N signifies that the element has no site preference in sublattice of Ni_3Al.

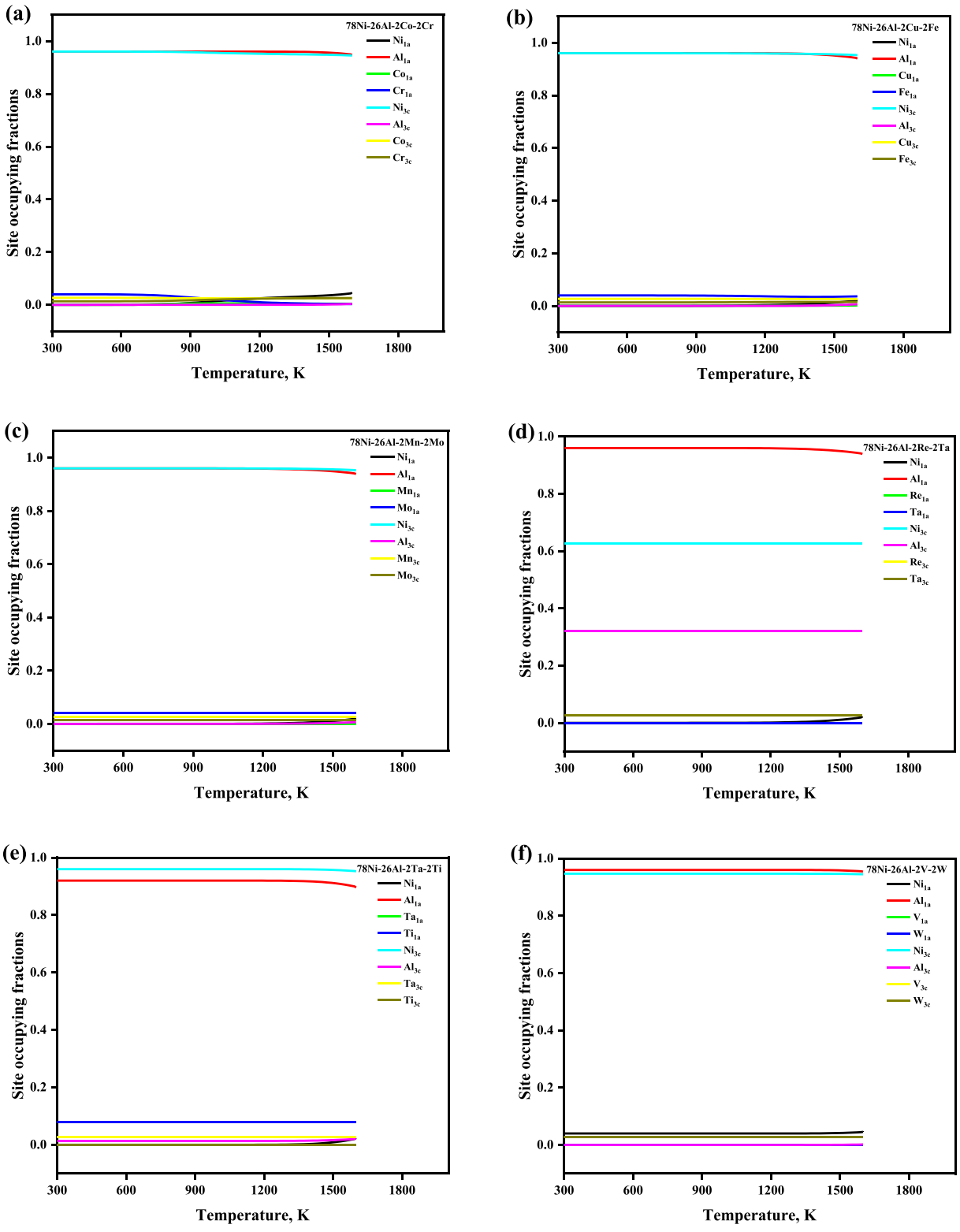

Fig. 7 The temperature- and composition-dependent SOFs of the alloying element in Ni_3Al-based γ′ phase with the composition 78Ni-26Al-2 M_1-2 M_2 which is normalized as 72.22Ni-24.08Al-1.85 M_1-1.85 M_2 (at. %).

range, while the site preferences of Cr, Fe, and Mo atoms are affected by the heat treatment. For example, when the heat treatment temperature is lower than 700 K, then Cr, Fe, and Mo atoms randomly occupied both the sublattices i.e., 1a and 3c, but preferred to occupy the 1a sublattice. When the heat treatment temperature is higher than 1273 K, then Fe, and Mo atoms preferred the 1a sublattice, and all Cr atoms preferred the 3c sublattice exclusively. The temperature-

Table 3 The predicted site preference at selective low and high temperatures for detailed comparison.

Compositions	Elements	Site occupying fractions (SOFs)					
		at 298 K			at 1273 K		
		1a	3c	Preferred	1a	3c	Preferred
$Ni_{75}Al_{25}$	Ni	0	1	3c	0.0015	0.9994	3c
	Al	1	0	1a	0.9984	0	1a
$Co_{75}Al_{25}$	Co	0	1	3c	0.7409	0.7530	3c
	Al	1	0	1a	0.2590	0.2469	1a
$Ni_{72}Al_{28}$	Ni	0	1	3c	0	0.9599	3c
	Al	1	0	1a	1	0.0401	1a
$Ni_{78}Al_{22}$	Ni	0.1199	1	3c	0.1200	0.9999	3c
	Al	0.8800	0	1a	0.8799	0	1a
$Ni_{78}Al_{26}Co_4$	Ni	0	0.9600	3c	0.0285	0.9504	3c
	Al	1	0	1a	0.9598	0	1a
	Co	0	0.0400	3c	0.0115	0.0494	3c
$Ni_{78}Al_{26}Cr_4$	Ni	0	0.9600	3c	0.0285	0.9504	3c
	Al	0.9600	0	1a	0.9597	0	1a
	Cr	0.0400	0.0400	both	0.0116	0.0494	3c
$Ni_{78}Al_{26}Cu_4$	Ni	0	0.9600	3c	0.0314	0.9495	3c
	Al	0.9600	0	1a	0.9598	0	1a
	Cu	0.0400	0.0400	both	0.0086	0.0504	3c
$Ni_{78}Al_{26}Fe_4$	Ni	0	0.9600	3c	0.0015	0.9594	3c
	Al	0.9600	0	1a	0.9578	0	1a
	Fe	0.0400	0.0400	both	0.0405	0.0398	1a
$Ni_{78}Al_{26}Mn_4$	Ni	0.0398	0.9467	3c	0.0401	0.9466	3c
	Al	0.9600	0	1a	0.9598	0	1a
	Mn	0	0.0532	3c	0	0.0533	3c
$Ni_{78}Al_{26}Mo_4$	Ni	0	0.9600	3c	0	0.9600	3c
	Al	0.9202	0.0130	1a	0.9200	0.0133	1a
	Mo	0.0798	0.0267	1a	0.0799	0.0267	1a
$Ni_{78}Al_{26}Re_4$	Ni	0.0197	0.9534	3c	0.0401	0.9466	3c
	Al	0.9600	0	1a	0.9598	0	1a
	Re	0.0202	0.0465	3c	0	0.0533	3c
$Ni_{78}Al_{26}Ta_4$	Ni	0	0.9600	3c	0	0.9599	3c
	Al	0.9600	0	1a	0.9298	0.0100	1a
	Ta	0.0400	0.0400	both	0.0700	0.0299	1a
$Ni_{78}Al_{26}Ti_4$	Ni	0.2247	0.8753	3c	0.0400	0.9466	3c
	Al	0.7752	0.0713	1a	0.9599	0	1a
	Ti	0	0.0533	3c	0	0.0533	3c
$Ni_{78}Al_{26}V_4$	Ni	0	0.9600	3c	0	0.9599	3c
	Al	0.9600	0	1a	0.8401	0.0399	1a
	V	0.0400	0.0400	both	0.1597	0	1a
$Ni_{78}Al_{26}W_4$	Ni	0	0.9599	3c	0.0362	0.9479	3c
	Al	0.9600	0	1a	0.9598	0	1a
	W	0.0399	0.0400	3c	0.0038	0.0520	3c
$Ni_{78}Al_{26}Co_2Cr_2$	Ni	0	0.9600	3c	0.0277	0.9508	3c
	Al	0.9600	0	1a	0.9598	0	1a
	Co	0	0.0267	3c	0.0050	0.0250	3c
	Cr	0.0400	0.0133	1a	0.0075	0.0242	3c
$Ni_{78}Al_{26}Cu_2Fe_2$	Ni	0	0.9600	3c	0.0046	0.9585	3c
	Al	0.9600	0	1a	0.9592	0	1a
	Cu	0	0.0267	3c	0	0.0264	3c
	Fe	0.0400	0.0133	1a	0.0354	0.0149	1a
$Ni_{78}Al_{26}Mn_2Mo_2$	Ni	0	0.9600	3c	0.0020	0.9593	3c
	Al	0.9600	0	1a	0.9581	0	1a
	Mn	0	0.0267	3c	0	0.0267	3c
	Mo	0.0400	0.0133	1a	0.0399	0.0134	1a
$Ni_{78}Al_{26}Re_2Ta_2$	Ni	0	0.6266	3c	0.0019	0.6268	3c
	Al	0.9999	0.3200	1a	0.9581	0.33	1a
	Re	0	0.0266	3c	0	0.0267	3c
	Ta	0	0.0266	3c	0	0.0267	3c
$Ni_{78}Al_{26}Ta_2Ti_2$	Ni	0	0.9600	3c	0	0.9598	3c
	Al	0.9200	0.0133	1a	0.9295	0.0134	1a
	Ta	0	0.0266	3c	0	0.0266	3c

(*continued on next page*)

Table 3 (*continued*)

Compositions	Elements	Site occupying fractions (SOFs)					
		at 298 K			at 1273 K		
		1a	3c	Preferred	1a	3c	Preferred
$Ni_{78}Al_{26}V_2W_2$	Ti	0.0800	0	1a	0.08	0	1a
	Ni	0.0400	0.9466	3c	0.0400	0.9466	3c
	Al	0.9600	0	1a	0.9599	0	1a
	V	0	0.0266	3c	0	0.0266	3c
	W	0	0.0267	3c	0	0.0267	3c

dependent thermodynamic functions of the quaternary system with the composition 78Ni-26Al-2 M_1-2 M_2 are shown in Fig. 8, and we have observed that ΔG_{mix}, ΔH_{mix}, and ΔS_{mix} are decreasing with the increase of the heat treatment, and configurational entropy S_{conf} is increasing with the increase of the temperature, which shows that the doping of quaternary elements also enhances the structural stability, respectively. The calculated site preference for stoichiometric, and nonstoichiometric Ni_3Al, stoichiometric Co_3Al along with ternary and quaternary systems at selective low and high temperatures was given in Table 3 for comparison conveniently.

3.3. Graphical demonstration of atoms distribution on the sublattice

Based on the calculated SOFs, the atom distributions on the sublattice and thus on the full lattice were graphically demonstrated for an intuitive understanding of the tendency of site preference. The site occupying fraction of FCC_$L1_2$ structure alloys 75Ni-25Al with unit cell and supercell is shown in Fig. 9, where a 10 × 10 × 10 supercell has been built based on AB_3_$L1_2$ crystal lattice structure, and the distribution of atoms on the sublattice and thus on the full lattice were shown

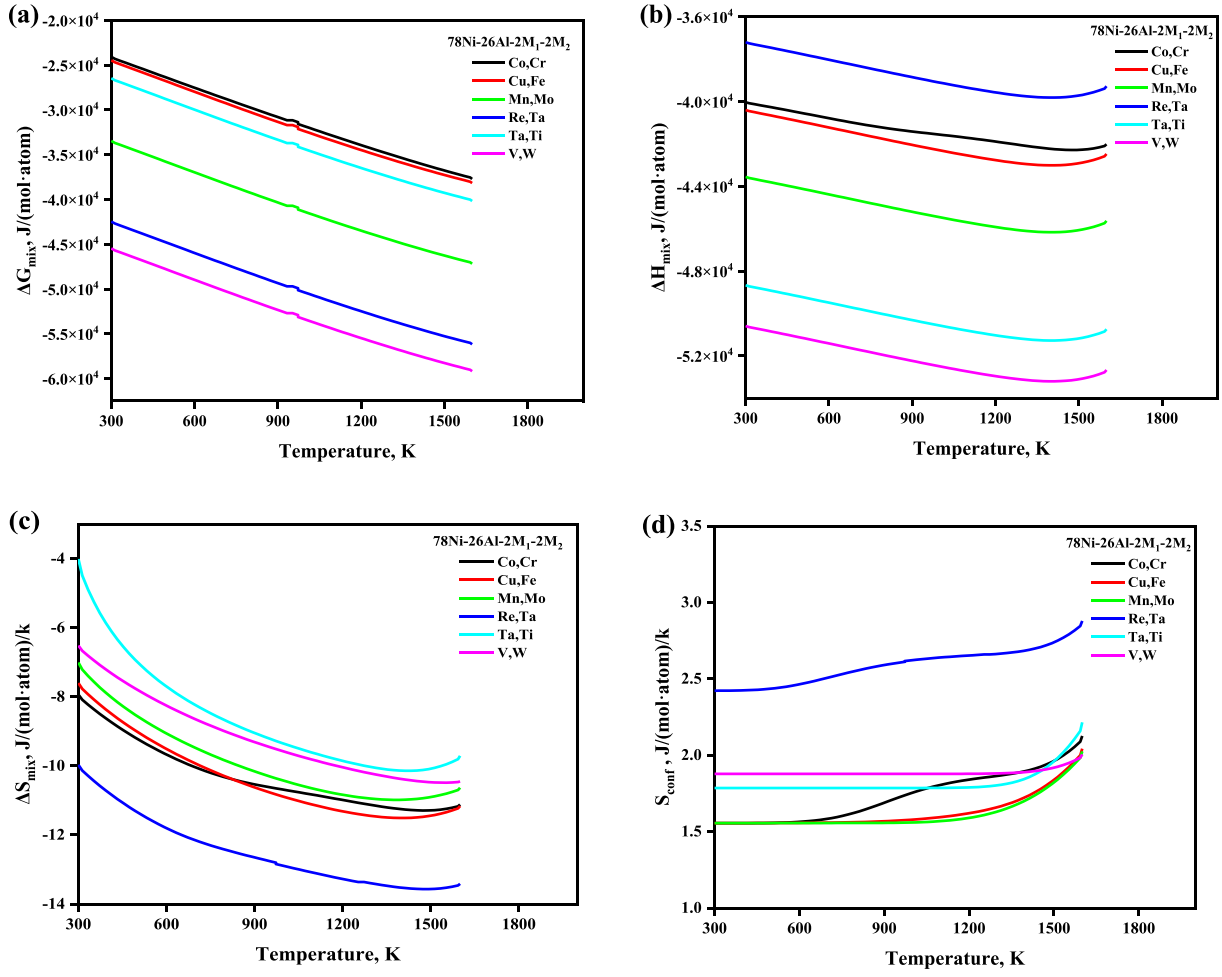

Fig. 8 The temperature- and composition-dependent thermodynamic functions of the alloying element in Ni_3Al-based γ′ phase with the composition 78Ni-26Al-2 M_1-2 M_2 which is normalized as 72.22Ni-24.08Al-1.85 M_1-1.85 M_2 (at. %).

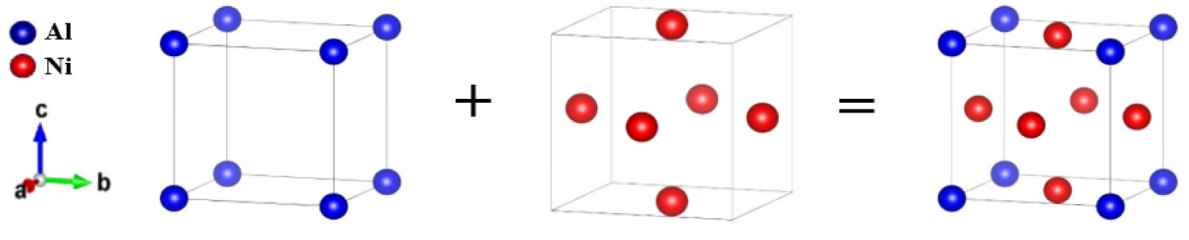

(a)

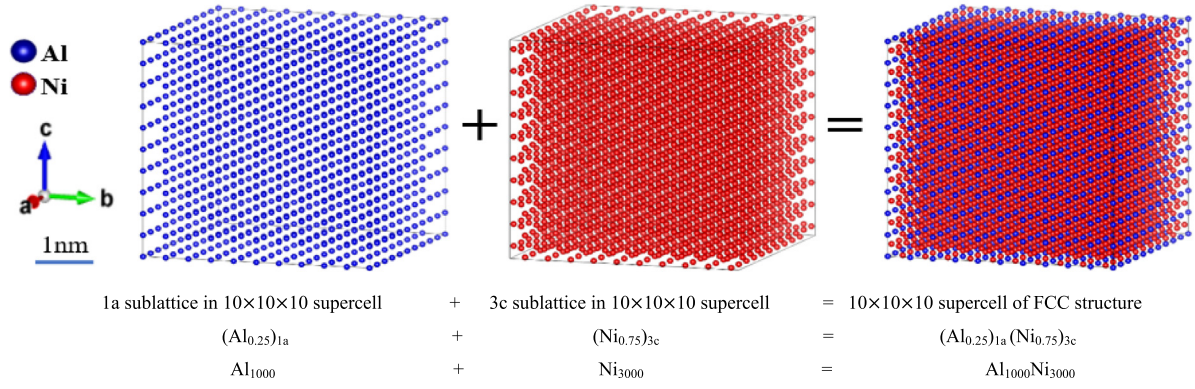

(b)

Fig. 9 Visualization of the atomic distribution of the stoichiometric Ni_3Al γ' phase with the real relative size bar on the sublattice 1a and 3c based on a $10 \times 10 \times 10$ supercell of the FCC_$L1_2$ (a) unit-cell of pure stoichiometric Ni_3Al (b) ordered structure at room temperature.

in a statistical sense. The supercell has 4000 atoms, including 1000 atoms on 1a sublattice and 3000 atoms on 3c sublattice. In this study, the estimated SOFs were used to account for the integer numbers of distinct atoms on each sort of sublattice. Here we relatively assumed that the atoms occupy each type of sublattices randomly for the calculated integer numbers, so for a specific configuration, the distribution of atoms in each type of sublattice and whole lattice may be visually represented. Similarly, we have built a $10 \times 10 \times 10$ supercell for a better view of the atom distribution (4000 atoms in total) for the alloying composition 72Ni-24Al-4 W. In order to fulfill further calculations concerning the lattice distortion, thermodynamic properties, and mechanical properties based on the available computing resources, a $3 \times 3 \times 3$ supercell containing 108 atoms was also built, and 1a and 3c sublattices were separated and nested in Fig. 10, thus an applied structure file (POSCAR) was prepared. So, we reasonably described the distribution of the atoms on sublattice and thus on a crystal lattice, which is one of the most essential structural information.

3.4. Alloying effects on mechanical and thermodynamic properties

To explore the effect of the alloying elements on the mechanical properties, the elasticity was calculated at the ground state i.e., 0 K. Because it relates to the key characteristics of the mechanical properties of materials such as the stability of the mechanical structure, brittleness, stiffness, hardness, strength, fracture toughness (Chen and Bielawski, 2008), and interatomic bonding (Pugh and Xcii., 1954; Nye, 1985). Table 4 summarizes the elastic modulus calculation findings., which reveal that the elastic properties of pure Ni_3Al agree well with the theoretical (Kim et al., 2010; Wu and Li, 2012; Xu et al., 2013; Xu et al., 2018) as well as experimental (Kayser and Stassis, 1981; Prikhodko et al., 1999; Chen and Knowles, 2003) data available in the literature. For the reliability of our calculations, the elastic properties of pure Co_3Al are also summarized in Table 4 by implementing the same methodology, and the present results agree well with other available calculated (Xu et al., 2013; Xu et al., 2018) and experimental data (Kayser and Stassis, 1981; Prikhodko et al., 1999). The results showed that all the alloying elements would enhance the bulk

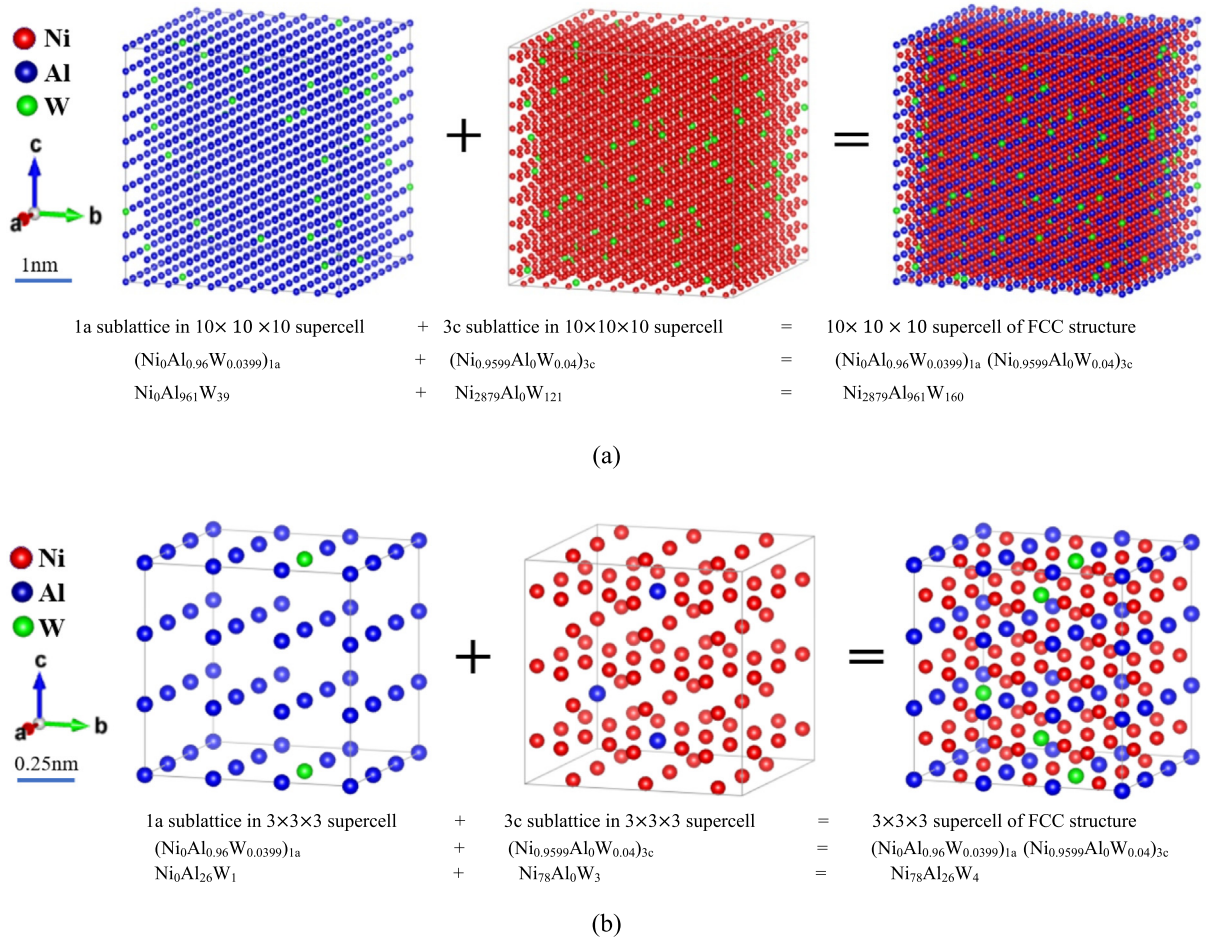

Fig. 10 Atomic site occupancy configuration of FCC_$L1_2$ structure alloys 72Ni-24Al-4 W with the real relative size bar based on a different dimension of the FCC_$L1_2$ supercell at room temperature (a) 10 × 10 × 10 (b) 3 × 3 × 3 supercell.

modulus of polycrystalline Ni_3Al alloys except Mn, Mo, and Ti, in which Mn have the greatest influence on reducing the bulk and shear modulus of Ni_3Al. Additionally, we employed the mechanical stability criteria (Born, 1939) i.e., $C_{11} > 0$, $C_{44} > 0$, $C_{11} > |C_{12}|$, $(C_{11} + 2C_{12}) > 0$ to examine the mechanical stability of superalloys. It is noted that the additional alloying M_i elements have a significant effect on the elastic constants, but they fulfill the mechanical stability criteria which show that they are mechanically stable.

To study the ductile and brittle behavior of materials, we computed the bulk to shear modulus ratio (B/G ratio) proposed by Pugh (Pugh and Xcii., 1954). A material is ductile if the ratio is higher than 1.75, and if it's lower than 1.75 then the material is brittle, our calculated results showed that all Ni_3Al alloys are ductile in nature because their B/G ratios are higher than 1.75. Thus, these alloying elements might be utilized as a precipitate to increase superalloy toughness. Furthermore, we calculated the tetragonal shear modulus $C' = (C_{11} - C_{12})/2$ and Cauchy pressure $(C_{12} - C_{44})$ (Pettifor, 1992) to examine the bonding nature. A positive Cauchy pressure specifies a ductile behavior and metallic bonding, while a negative one implies angular character and covalent bonding. Additionally, the toughness of materials is more stable with higher Cauchy pressure. Evidently, the Cauchy pressures of all additional alloying elements have positive values, suggesting their toughness and metallic characteristics, as shown in Table 4. It can be seen from Table 4 that the addition of impurity elements increases the Cauchy pressure of the alloy, indicating that the addition of some alloy elements to the alloy system can increase the plasticity of the alloy. In addition to $Ni_{78}Al_{26}Cr_4$, the Poisson's ratio and B/G ratio, which judged the ductility of materials, also show the same results, but the addition of impurity elements will reduce the shear modulus of the system. The shear modulus is based on the C_{44} value and is used to measure the resistance of solids to shape change, the smaller its value, the weaker its resistance to shape change, which results in increased its plasticity, which is consistent with the results of Cauchy pressure, Poisson's ratio, and B/G value. Except for $Ni_{78}Al_{26}Cr_4$, the addition of impurity elements reduces the young's modulus of the system, which is an index to measure the stiffness of materials. We can conclude that the addition of some impurity elements will reduce the stiffness of the system, which also indicates that its resistance to elastic deformation decreases.

Furthermore, we also calculated the microhardness $H = (1 - 2\nu)E/6(1+\nu)$ (Cheng et al., 2013) which is the key characteristic of solid materials that gives information about the wear resistance to permanent or plastic deformation. It is often assumed that the higher the material's hardness, the better the wear resistance. According to our calculations, we

have observed that Cr doping can increase the microhardness of Ni_3Al alloys, and has a significant effect because its microhardness is the largest (12.77 GPa) among other additional alloying elements, so it possesses the best wear resistance. Additionally, hardness is often correlated with bond energy. It's also worth noting that materials with high hardness have a high bond strength, implying that Cr doping has a highest average bond energy (Sun et al., 2020). To deeply understand the relationship between macroscopic properties and the microscopic mechanism of alloys, we have calculated the bond energy of some selective alloying elements. For this purpose, firstly, we built a 15 × 15 × 15 (Å) cubic cell, then placed atoms into the cube to only optimized the atomic position, and then extract the total energy from the output file as the bond energy. For example, we calculated the bond energies of the pure elements Al (-0.247) and Ni (-0.343) in eV/atom, and the calculated bond energies of all compositions involved in this work are $Ni_{78}Al_{26}Co_4$ (-6.322), $Ni_{78}Al_{26}Cr_4$ (-6.613), $Ni_{78}Al_{26}Cu_4$ (-6.464), $Ni_{78}Al_{26}Fe_4$ (-6.469), $Ni_{78}Al_{26}Mn_4$ (-6.452), $Ni_{78}Al_{26}Mo_4$ (-6.480), $Ni_{78}Al_{26}Re_4$ (-6.483), $Ni_{78}Al_{26}Ta_4$ (-6.470), $Ni_{78}Al_{26}Ti_4$ (-6.472), $Ni_{78}Al_{26}V_4$ (-6.493), and $Ni_{78}Al_{26}W_4$ (-6.446) in eV/atom, respectively. We have observed that the bond energy of $Ni_{78}Al_{26}Cr_4$ is the minimum among other compositions which showed that it has the highest hardness, which corresponds to our calculated results. In addition, the calculated crystal lattice parameters of doped Ni_3Al-based γ' phase alloys involved in this work are summarized in Table 5.

Furthermore, to consider the relationship between the density of states (DOS) and mechanical properties, we have calcu-

Table 4 Calculated independent elastic constants C_{ij} (GPa), tetragonal shear modulus C' (GPa), Cauchy pressure $C_{12} - C_{44}$ (GPa), bulk modulus B (GPa), shear modulus G (GPa), Young's modulus E (GPa), Poisson's ratio v, microhardness H (GPa), bulk modulus to shear modulus ratio B/G.

Alloys	C_{11}	C_{12}	C_{44}	C'	$C_{12} - C_{44}$	B	G	E	v	H	B/G
Ni_3Al	238.85	146.07	126.61	46.39	19.46	176.98	84.68	219.10	0.29	11.65	2.09
Calc. (Kim et al., 2010)	242.2	151.8	125.4	–	–	182.0	83.0	217.	–	–	2.18
Calc. (Wu and Li, 2012)	243.8	148.7	123.4	–	–	180.4	84.2	218.5	–	–	2.14
Calc. (Xu et al., 2013)	231.0	152.2	120.2	–	–	178.5	76.9	201.8	0.31	–	2.32
Calc. (Xu et al., 2018)	232.7	151.4	120.6	–	–	178.5	78.1	204.4	0.31	–	2.29
Expt. (Kayser and Stassis, 1981)	224.0	148.0	125.0	–	–	173.3	77.7	202.9	031	–	2.23
Expt. (Prikhodko et al., 1999)	224.5	148.6	124.4	–	–	173.9	77.5	202.3	0.31	–	2.24
Expt. (Chen and Knowles, 2003)	225	149	124	–	–	174	77	202	–	–	2.26
Co_3Al	211.93	196.24	96.23	7.85	100.01	201.47	39.18	110.37	0.41	2.38	5.14
Calc. (Xu et al., 2013)	205.7	179.5	92.7	–	–	188.2	44.0	113.3	0.39	–	4.28
Calc. (Xu et al., 2018)	218.5	194.8	92.1	–	–	202.7	42.4	118.9	0.40	–	4.78
$Ni_{78}Al_{26}Co_4$	235.15	185.91	130.95	24.62	54.96	202.32	68.21	183.97	0.35	6.89	2.97
$Ni_{78}Al_{26}Cr_4$	258.30	137.23	115.48	60.54	21.75	177.58	89.11	229.03	0.29	12.77	1.99
$Ni_{78}Al_{26}Cu_4$	221.20	157.31	98.45	31.95	58.86	178.61	62.78	168.59	0.34	6.58	2.84
$Ni_{78}Al_{26}Fe_4$	224.40	163.59	120.58	30.41	43.01	183.86	69.83	185.95	0.33	7.85	2.63
$Ni_{78}Al_{26}Mn_4$	189.90	159.34	103.13	15.28	56.21	169.53	49.62	135.63	0.37	4.41	3.42
$Ni_{78}Al_{26}Mo_4$	201.84	158.58	111.52	21.63	47.06	173.00	58.73	158.27	0.35	5.97	2.95
$Ni_{78}Al_{26}Re_4$	242.95	172.58	125.94	35.19	46.64	196.04	75.81	201.47	0.33	8.66	2.59
$Ni_{78}Al_{26}Ta_4$	230.59	172.80	122.90	28.90	49.90	192.06	69.35	185.70	0.34	7.45	2.77
$Ni_{78}Al_{26}Ti_4$	218.59	148.20	92.50	35.19	55.70	171.66	62.80	167.92	0.34	6.83	2.73
$Ni_{78}Al_{26}V_4$	227.56	161.87	131.90	32.85	29.97	183.77	76.03	200.45	0.32	9.21	2.42
$Ni_{78}Al_{26}W_4$	216.37	168.87	121.24	23.75	47.63	184.70	64.07	172.28	0.34	6.64	2.88

Table 5 The calculated crystal lattice parameters of fully relaxed* doped Ni_3Al-based γ' phase alloys.

Alloys	a(Å)	b(Å)	c(Å)	α(°)	β(°)	γ(°)	V (Å^3)
Ni_3Al	10.73036	10.73036	10.73036	90.0000	90.0000	90.0000	1235.5007
Co_3Al	10.77142	10.80456	10.77487	90.1515	89.9816	90.1573	1253.9754
$Ni_{78}Al_{26}Co_4$	10.75576	10.75904	10.70553	89.9976	89.9864	90.0016	1238.8611
$Ni_{78}Al_{26}Cr_4$	10.79226	10.75047	10.72976	89.9533	90.1585	89.9371	1244.8800
$Ni_{78}Al_{26}Cu_4$	10.72994	10.79370	10.76744	90.0969	89.7926	90.0931	1247.0265
$Ni_{78}Al_{26}Fe_4$	10.71747	10.71747	10.71747	90.0000	90.0000	90.0000	1231.0520
$Ni_{78}Al_{26}Mn_4$	10.78957	10.75607	10.75665	90.0458	89.9412	89.9884	1248.3448
$Ni_{78}Al_{26}Mo_4$	10.74301	10.74301	10.74301	90.0000	90.0000	90.0000	1239.8746
$Ni_{78}Al_{26}Re_4$	10.66760	10.82554	10.71324	89.8878	89.8871	89.9994	1237.1876
$Ni_{78}Al_{26}Ta_4$	10.73043	10.76918	10.84262	90.0943	89.9925	89.9590	1252.9491
$Ni_{78}Al_{26}Ti_4$	10.70245	10.70245	10.70245	90.0000	90.0000	90.0000	1225.8830
$Ni_{78}Al_{26}V_4$	10.86879	10.48691	10.86796	89.7902	89.4979	89.9953	1238.6743
$Ni_{78}Al_{26}W_4$	10.75450	10.75450	10.75450	90.0000	90.0000	90.0000	1243.8587

*Fully relaxed: Volume, shape, and atom position are fully relaxed by setting ISIF = 3 and NSW = 10 in the INCAR file.

lated the DOS of pure Ni_3Al-based γ' phase with composition 75Ni-25Al (at. %), pure Co_3Al-based γ' phase with composition 75Co-25Al (at. %), and DOS of Ni_3Al doped with Co with composition 72Ni-24Al-4Co (at. %), here we take it as an example. From Fig. 11, it is evident that the range of DOS has been expanded in both the valence and conduction regions. The peak intensities have been decreased to make the DOS near Fermi-level flat slightly for all the compounds. According to the above analyses, the addition of the alloying elements (i.e., TMs) can effectively reduce the covalent nature of Ni_3Al-based γ' phase alloys, resulting in enhanced ductility, which is resembled to our calculated mechanical properties results.

Debye temperature Θ_D is used to observe the impact of alloying elements on the thermodynamic properties of Ni_3Al alloys. Besides indicating a specific shear modulus, elastic parameters, thermal conductivity, and melting temperature, the Debye temperature also signifies the stiffness of lattices. A high Debye temperature indicates strong interactions of atoms. The Debye temperature in terms of average sound velocity v_m can be obtained by (Lowrie, 1963):

$$\Theta_D = \frac{h}{k_B}\left[\frac{3N}{4\pi}\left(\frac{N_A\rho}{M}\right)\right]^{1/3} v_m \tag{17}$$

where, h, K_B, and N_A are Plank, Boltzmann, and Avogadro constants, ρ is the density of alloys, N is the number of atoms in a cell, and M is the molecular mass. v_m is given by (Anderson, 1963):

$$v_m = \left[\frac{1}{3}\left(\frac{2}{v_t^3} + \frac{1}{v_l^3}\right)\right]^{-\frac{1}{3}} \tag{18}$$

where v_t and v_l are the longitudinal and transverse elastic wave velocity. mt and ml can be deduced from Navier's equation (Schreiber et al., 1975):

$$v_l = \left[\left(\frac{3B + 4G}{3\rho}\right)\right]^{1/2} \text{and } v_t = \left(\frac{G}{\rho}\right)^{1/2} \tag{19}$$

The calculated results are listed in Table 6, which shows that only doping with Cr enhances the Debye temperature of Ni_3Al alloys remarkably, resulting in improved crystallographic interaction. Although there is no measured data Θ_D for composition 78Ni-26Al-4M_i available in the literature for

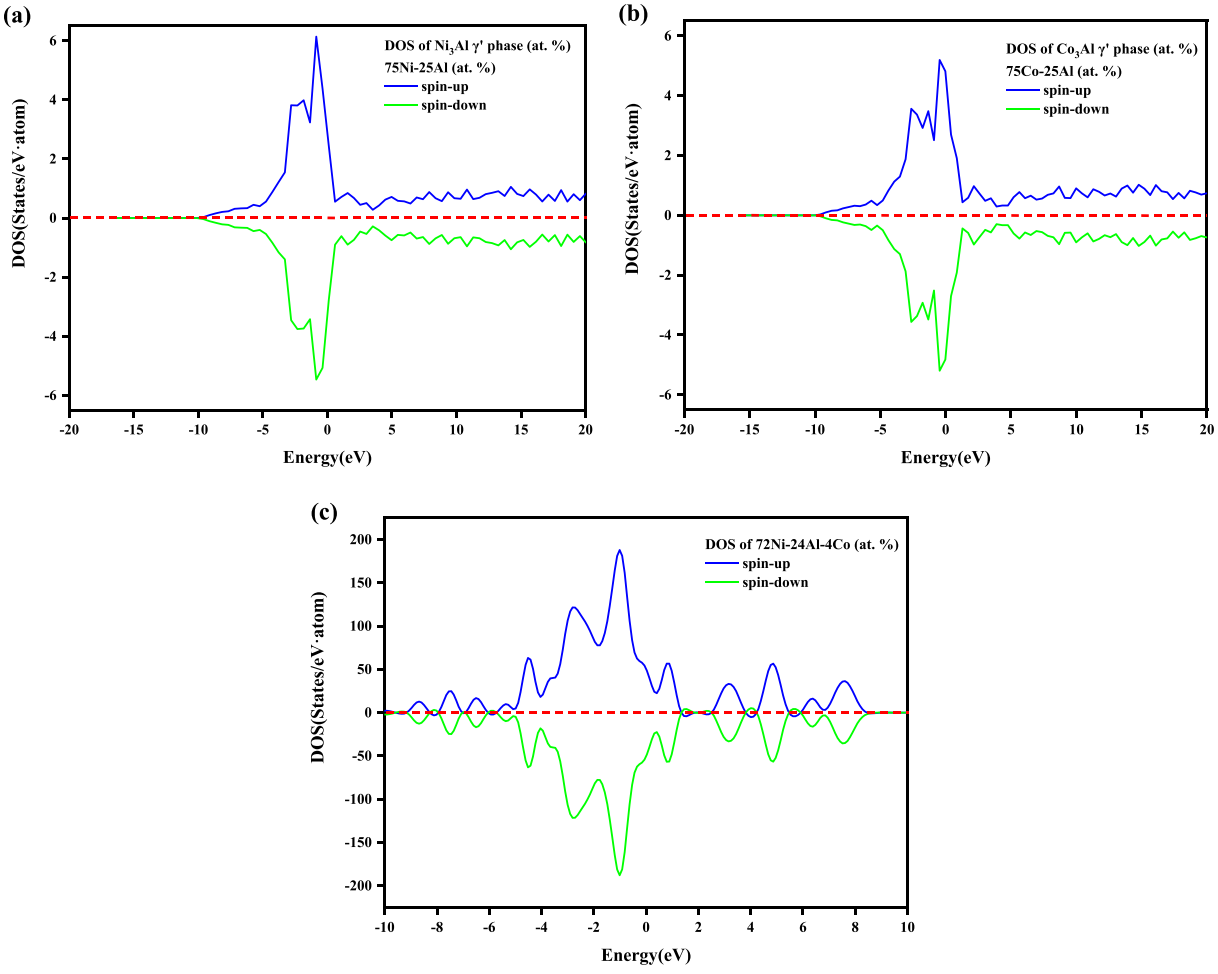

Fig. 11 Projected density of states of Ni_3Al-based γ' phase with different composition (at. %) (a) 75Ni-25Al (b) 75Co-25Al (c) 72Ni-24Al-4Co, at 0 GPa pressure. The DOS for spin-up and spin-down are plotted by the blue and green lines, respectively. The Fermi level has been subtracted to zero energy.

Table 6 Calculated transverse (v_t), longitudinal (v_l), average sound wave velocity (v_m) in (ms^{-1}) and Debye temperature (Θ_D, K).

Alloys	v_t	v_l	v_m	Θ_D
Ni_3Al	3235.89	6132.89	3617.69	478.60
Calc. (Xu et al., 2013)	3219.9	6147.4	3601.6	476.8
Expt. (Kayser and Stassis, 1981; Stassis et al., 1981)	3225.3 (Kayser and Stassis, 1981)	6102.6 (Kayser and Stassis, 1981)	3605.4 (Kayser and Stassis, 1981)	470 (Stassis et al., 1981)
$Ni_{78}Al_{26}Co_4$	3126.07	6481.86	3513.96	464.45
$Ni_{78}Al_{26}Cr_4$	3673.93	6700.42	4096.02	540.20
$Ni_{78}Al_{26}Cu_4$	2959.48	6049.35	3324.12	438.65
$Ni_{78}Al_{26}Fe_4$	3195.07	6363.13	3583.38	473.84
$Ni_{78}Al_{26}Mn_4$	2729.24	5948.06	3075.46	403.97
$Ni_{78}Al_{26}Mo_4$	2614.06	5407.51	2938.05	385.77
$Ni_{78}Al_{26}Re_4$	2410.36	4771.75	2702.32	356.50
$Ni_{78}Al_{26}Ta_4$	2326.01	4711.39	2611.25	344.68
$Ni_{78}Al_{26}Ti_4$	3133.10	6318.43	3516.45	463.60
$Ni_{78}Al_{26}V_4$	3395.21	6575.10	3801.24	502.45
$Ni_{78}Al_{26}W_4$	2231.72	4582.54	2507.32	330.16

comparative comparison, but based on the excellent agreement between the current study with other theoretical (Xu et al., 2013) and experimental (Kayser and Stassis, 1981; Stassis et al., 1981) results of Θ_D for Ni_3Al, it seems reasonable to conclude that the present theoretical results are valid for Ni_3Al superalloys alloyed with M_i, respectively.

4. Conclusions

The temperature- and composition-dependent site preferences were predicted concerning the binary, ternary, and quaternary Ni_3Al-based γ' phase with $L1_2$ structure alloyed with some frequently adopted transition metals M_i, where M_i represents Co, Cr, Cu, Fe, Mn, Mo, Re, Ta, Ti, V, and W atoms, using a two-sublattice thermodynamic model $(Ni, Al, M_i)_{1a}(Ni, Al, M_i)_{3c}$. It was revealed that for the stoichiometry binary Ni_3Al show a fully ordered structure at all temperatures. For the γ' phase with the composition 78Ni-26Al-4M_i, where xNi/x_{Al} = 3:1, Mo atoms always preferred to occupy the 1a sublattice (Al site), while Co, Mn, and Ti atoms always prefer the 3c sublattice (Ni site) in the whole temperature range, while the site preference of the alloying elements such as Cr, Cu, Fe, Re, Ta, Vlore W atom is affected by the heat treatment temperature. For example, when the heat treatment temperature is lower than 700 K, Cr, Cu, Fe, Ta, V, and W atoms occupy the 1a and 3c sublattice randomly, and Re atoms prefer to 3c sublattice, while when the heat treatment temperature is higher than 1273 K, Cr, Cu, Mo, and W atoms prefer 3c sublattice, Fe, Ta atoms prefer to 1a sublattice, while all Re atoms occupy 3c sublattice exclusively, and all V atoms occupy 1a sublattice exclusively, respectively. The site preference of the quaternary system with a selective composition 78Ni-26Al-2 M_1-2 M_2, has been also investigated. It is revealed that Co, Cu, Mn, Re, Ta, V, and W atoms prefer 3c sublattice (Ni site), Ti prefers 1a sublattice (Al site), in the whole temperature range, while the site preferences of Cr, Fe, and Mo atoms are affected by the heat treatment. For example, when the heat treatment temperature is lower than 700 K, Cr, Fe, and Mo atoms have no obvious site preference by randomly occupying both 1a sublattice and 3c sublattice, but slightly prefer to 1a sublattice. When the heat treatment temperature is higher than 1273 K, Fe, and Mo atoms prefer the 1a sublattice, and all Cr atoms occupy the 3c sublattice exclusively. Cr, Re, and V doping can improve the microhardness of Ni_3Al alloys; in particular, the effect of Cr is extraordinary; and all elements, except Mn, Mo, and Ti, would enhance the bulk modulus of Ni_3Al-based γ' phase, in which Mn have the greatest influence on reducing the bulk and shear modulus, respectively. All of the computed Ni_3Al alloys are all inherent ductile based on the Pugh criterion. Only Cr doping significantly enhances the Debye temperature of the Ni_3Al-based γ' phase. Our calculated results are highly consistent with the available literature. The quantitative understanding of the site preference and strengthening mechanisms are expected to promote the development of the novel Ni-based superalloy.

Declaration of Competing Interest

The authors declare that they have no known competing financial interests or personal relationships that could have appeared to influence the work reported in this paper.

Acknowledgments

This work is financially supported by the National Natural Science Foundation of China (50971043, 51171046, 21973012), Key Research and Development Program of China (2017YFB0701700, CISRI-21T62450ZD), Natural Science Foundation of Fujian Province (2021J01590, 2014J01176, 2018J01754, 2020J01474), National Key Laboratory of Eco-materials Advanced Technology (Fuzhou University), Student Research and Training Program (SRTP) of Fuzhou University (27297), State Administration for Market Regulation (2021MK050) and Fujian Provincial Department of Science & Technology (2021H6011).

Appendix A. Supplementary data

Supplementary data to this article can be found online at https://doi.org/10.1016/j.arabjc.2022.104278.

References

Abe, T., Sundman, B., Onodera, H., 2006. Thermodynamic assessment of the Cu–Pt system. Journal of Phase Equilibria and Diffusion 27 (1), 5–13.

Ali, H., 2022. Materials Today Communications 33, 104447. The ordering behavior of Co3Al-based γ′ phase with L12 structure predicted by the thermodynamic model with support of first-principles calculations.
Amouyal, Y., Mao, Z., Booth-Morrison, C., Seidman, D.N., 2009. On the interplay between tungsten and tantalum atoms in Ni-based superalloys: An atom-probe tomographic and first-principles study. Appl. Phys. Lett. 94, (4) 041917.
Amouyal, Y., Mao, Z., Seidman, D.N., 2010. Effects of tantalum on the partitioning of tungsten between the γ-and γ′-phases in nickel-based superalloys: Linking experimental and computational approaches. Acta Mater. 58 (18), 5898–5911.
Amouyal, Y., Mao, Z., Seidman, D.N., 2014. Combined atom probe tomography and first-principles calculations for studying atomistic interactions between tungsten and tantalum in nickel-based alloys. Acta Mater. 74, 296–308.
Anderson, O.L., 1963. A simplified method for calculating the Debye temperature from elastic constants. J. Phys. Chem. Solids 24 (7), 909–917.
Andersson, J.-O., Helander, T., Höglund, L., Shi, P., Sundman, B., 2002. Thermo-Calc & DICTRA, computational tools for materials science. Calphad 26 (2), 273–312.
Bagot, P.A., Silk, O., Douglas, J., Pedrazzini, S., Crudden, D., Martin, T., Hardy, M., Moody, M.P., Reed, R.C., 2017. An Atom Probe Tomography study of site preference and partitioning in a nickel-based superalloy. Acta Mater. 125, 156–165.
Baroni, S., de Gironcoli, S., Dal Corso, A., Giannozzi, P., 2001. Phonons and related crystal properties from density-functional perturbation theory. Rev. Mod. Phys 73, 515.
Baroni, S., De Gironcoli, S., Dal Corso, A., Giannozzi, P., 2001. Phonons and related crystal properties from density-functional perturbation theory. Rev. Mod. Phys. 73 (2), 515.
Baroni, S., Giannozzi, P., Isaev, E., 2010. Density-functional perturbation theory for quasi-harmonic calculations. Rev. Mineral. Geochem. 71 (1), 39–57.
Barrett, C., Miner, R., Hull, D., 1983. The effects of Cr, Al, Ti, Mo, W, Ta, and Cb on the cyclic oxidation behavior of cast Ni-base superalloys at 1100 and 1150 C. Oxid. Met. 20 (5), 255–278.
Bensch, M., Preußner, J., Hüttner, R., Obigodi, G., Virtanen, S., Gabel, J., Glatzel, U., 2010. Modelling and analysis of the oxidation influence on creep behaviour of thin-walled structures of the single-crystal nickel-base superalloy René N5 at 980 ℃. Acta Mater. 58 (5), 1607–1617.
Blavette, D., Bostel, A., 1984. Phase composition and long range order in γ′ phase of a nickel base single crystal superalloy CMSX2: An atom probe study. Acta Metall. 32 (5), 811–816.
Blavette, D., Cadel, E., Pareige, C., Deconihout, B., Caron, P., 2007. Phase transformation and segregation to lattice defects in Ni-base superalloys. Microsc. Microanal. 13 (6), 464–483.
Blöchl, P.E., 1994. Projector augmented-wave method. Phys. Rev. B 50 (24), 17953.
Booth-Morrison, C., Mao, Z., Noebe, R.D., Seidman, D.N., 2008. Chromium and tantalum site substitution patterns in Ni_3Al ($L1_2$) γ′-precipitates. Appl. Phys. Lett. 93, (3) 033103.
Born, M., 1939. Thermodynamics of crystals and melting. J. Chem. Phys. 7 (8), 591–603.
Brimhall, J., Kissinger, H., Charlot, L., 1983. Amorphous phase formation in irradiated intermetallic compounds. Radiation Effects 77 (3–4), 273–293.
Broderick, S.R., Kumar, A., Oni, A.A., LeBeau, J.M., Sinnott, S.B., Rajan, K., 2018. Discovering chemical site occupancy-modulus correlations in Ni based intermetallics via statistical learning methods. Comput. Condens. Matter 14, 8–14.
Brooks, C.R., 1988. Heat Treatment Microstructure and Properties of Nonferrous Alloys. Metallurgical Industry Press 32.
Caron, P., Khan, T., 1999. Evolution of Ni-based superalloys for single crystal gas turbine blade applications. Aerosp. Sci. Technol. 3 (8), 513–523.
Chaudhari, M., Singh, A., Gopal, P., Nag, S., Viswanathan, G., Tiley, J., Banerjee, R., Du, J., 2012. Site occupancy of chromium in the γ′-Ni_3Al phase of nickel-based superalloys: a combined 3D atom probe and first-principles study. Philos. Mag. Lett. 92 (9), 495–506.
Chaudhari, M., Tiley, J., Banerjee, R., Du, J., 2013. Site preference and interaction energies of Co and Cr in gamma prime Ni_3Al: a first-principles study. Modell. Simul. Mater. Sci. Eng. 21, (5) 055006.
Chen, K., Bielawski, M., 2008. Interfacial fracture toughness of transition metal nitrides. Surf. Coat. Technol. 203 (5–7), 598–601.
Chen, S.-L., Daniel, S., Zhang, F., Chang, Y., Yan, X.-Y., Xie, F.-Y., Schmid-Fetzer, R., Oates, W., 2002. The PANDAT software package and its applications. Calphad 26 (2), 175–188.
Chen, Y., He, S., Yi, Z., Peng, P., 2019. A synergistic reinforcement of Re and W for ideal shear strengths of γ′-Ni_3Al phases. J. Phys. Chem. Solids 131, 34–43.
Chen, Q., Knowles, D.M., 2003. Mechanism of < 1 1 2 > /3 slip initiation and anisotropy of γ′ phase in CMSX-4 during creep at 750℃ and 750 MPa. Mater. Sci. Eng., A 356 (1–2), 352–367.
Chen, S., Pan, Y., 2022. Enhancing catalytic properties of noble metal@ MoS2/WS2 heterojunction for the hydrogen evolution reaction. Appl. Surf. Sci. 591, 153168.
Cheng, H.-C., Yu, C.-F., Chen, W.-H., 2013. First-principles density functional calculation of mechanical, thermodynamic and electronic properties of CuIn and Cu_2In crystals. J. Alloy. Compd. 546, 286–295.
Chiba, A., Hanada, S., Watanabe, S., 1991. Ductilization of Ni_3Al by macroalloying with Pd. Acta Metall.et materialia 39 (8), 1799–1805.
Chiba, A., Hanada, S., Watanabe, S., 1991. Effect of γ and γ′ former doping on ductility of Ni_3Al. Scr. Metall.et materialia 25 (2), 303–307.
Chiba, A., Hanada, S., Watanabe, S., 1992. Ductilization of Ni3 by microalloying with Ag. Scr. Metall.et materialia 26 (7), 1031–1036.
Cui, J.J., Sun, F., Zhang, J.X., 2012. Site preference of refractory elements in Ni-based single-crystal Superalloys alloying with Ru: from first principles. Trans Tech Publ, Advanced Materials Research, pp. 3–12.
Darolia, R., Lewandowski, J.J., Liu, C., Martin, P., Miracle, D., Nathal, M., 1993. Structural intermetallics, Warrendale, PA (United States). Metals and Materials Society, Minerals.
Ding, Q., Lao, Z., Wei, H., Li, J., Bei, H., Zhang, Z., 2020. Site occupancy of alloying elements in γ′ phase of nickel-base single crystal superalloys. Intermetallics 121, 106772.
Enomoto, M., Harada, H., 1989. Analysis of γ′/γ equilibrium in Ni−Al−X alloys by the. Metall. Trans. A 20 (4), 649–664.
Eriş, R., Mekhrabov, A.O., Akdeniz, M.V., 2017. High-temperature site preference and atomic short-range ordering characteristics of ternary alloying elements in γ′-Ni_3Al intermetallics. Phil. Mag. 97 (29), 2615–2631.
Eriş, R., Akdeniz, M.V., Mekhrabov, A.O., 2021. The Site Preferences of Transition Elements and Their Synergistic Effects on the Bonding Strengthening and Structural Stability of γ′-Ni_3 Al Precipitates in Ni-Based Superalloys: A First-Principles Investigation. Metallurgical and Materials Transactions A 52 (6), 2298–2313.
Fast, L., Wills, J., Johansson, B., Eriksson, O., 1995. Elastic constants of hexagonal transition metals: Theory. Phys. Rev. B 51 (24), 17431.
Gariboldi, E., Cabibbo, M., Spigarelli, S., Ripamonti, D., 2008. Investigation on precipitation phenomena of Ni–22Cr–12Co–9Mo alloy aged and crept at high temperature. Int. J. Press. Vessels Pip. 85 (1–2), 63–71.
Garimella, N., Ode, M., Ikeda, M., Murakami, H., Sohn, Y., 2008. Effects of Ir or Ta alloying addition on interdiffusion of $L1_2$–Ni_3Al. Intermetallics 16 (9), 1095–1103.

Geng, C., Wang, C., Yu, T., 2004. Site preference and alloying effect of platinum group metals in γ' -Ni_3Al. Acta Mater. 52 (18), 5427–5433.

Gleeson, B., Wang, W., Hayashi, S., Sordelet, D.J., 2004. Effects of platinum on the interdiffusion and oxidation behavior of Ni-Al-based alloys. Trans Tech Publ, Materials Science Forum, pp. 213–222.

Golberg, D., Demura, M., Hirano, T., 1999. Structure and yield strength of directionally solidified Ni3Al intermetallic premelted with $MoSi_2$ phase. Intermetallics 7 (1), 109–114.

Gong, W., Zhao, W., Miao, N., Zhou, J., Sun, Z., Li, S., Gong, S., 2018. Strengthening effects of alloying elements W and Re on Ni_3Al: A first-principles study. Comput. Mater. Sci. 144, 23–31.

Guard, W.J., 1959. Site Preference of Ternary Additions in Ni_3Si. Metall Soc AIME 2, 215–810.

Hono, K., Numakura, H., Szabo, I., Chiba, A., Sakurai, T., 1992. Determination of site preference of Cu and Ge in Ni_3Al. Surf. Sci. 266 (1–3), 358–363.

Horita, Z., Matsumura, S., Baba, T., 1995. General formulation for ALCHEMI. Ultramicroscopy 58 (3–4), 327–335.

Hu, K., Huang, J., Wei, Z., Peng, Q., Xie, Z., Sa, B., Wu, B., 2017. Elastic and thermodynamic properties of the Ti_2AlNb orthorhombic phase from first-principles calculations, physica status solidi (b) 254 (6), 1600634.

Huang, Y., Mao, Z., Noebe, R.D., Seidman, D.N., 2016. The effects of refractory elements on Ni-excesses and Ni-depletions at γ (fcc)/γ' ($L1_2$) interfaces in model Ni-based superalloys: Atom-probe tomographic experiments and first-principles calculations. Acta Mater. 121, 288–298.

Hung, L., Nastasi, M.G., J. and Mayer, JW Appl,, 1983. Phys. Lett 42, 672.

Inoue, M., Suganuma, K., Niihara, K., 1998. Toughening mechanism of Ni_3Al alloys by B-doping. J. Mater. Sci. Lett. 17 (23), 1967–1969.

Ivanov, E., Grigorieva, T., Golubkova, G., Boldyrev, V., Fasman, A., Mikhailenko, S., Kalinina, O., 1988. Synthesis of nickel aluminides by mechanical alloying. Mater. Lett. 7 (1–2), 51–54.

Jain, A., Shin, Y., Persson, K.A., 2016. Computational predictions of energy materials using density functional theory. Nat. Rev. Mater. 1 (1), 1–13.

Jiang, C., Sordelet, D., Gleeson, B., 2006. Site preference of ternary alloying elements in Ni_3Al: A first-principles study. Acta Mater. 54 (4), 1147–1154.

Jinlong, Y., Chuanyun, X., Shangda, X., Kelin, W., 1993. Site preference of alloying additions in intermetallic compounds. J. Phys.: Condens. Matter 5 (36), 6653.

Kayser, F., Stassis, C., 1981. The elastic constants of Ni_3Al at 0 and 23.5 ℃, Physica status solidi (a) 64 (1), 335–342.

Kim, D., Shang, S., Liu, Z., 2010. Effects of alloying elements on elastic properties of Ni_3Al by first-principles calculations. Intermetallics 18 (6), 1163–1171.

Kim, D., Shang, S.-L., Liu, Z.-K., 2012. Effects of alloying elements on thermal expansions of γ-Ni and γ'-Ni_3Al by first-principles calculations. Acta Mater. 60 (4), 1846–1856.

Kovarik, L., Unocic, R.R., Li, J., Sarosi, P., Shen, C., Wang, Y., Mills, M.J., 2009. Microtwinning and other shearing mechanisms at intermediate temperatures in Ni-based superalloys. Prog. Mater Sci. 54 (6), 839–873.

Kresse, G., Furthmüller, J., 1996. Efficient iterative schemes for ab initio total-energy calculations using a plane-wave basis set. Phys. Rev. B 54 (16), 11169.

Kresse, G., Joubert, D., 1999. From ultrasoft pseudopotentials to the projector augmented-wave method. Phys. Rev. B 59 (3), 1758.

Kumar, A., Chernatynskiy, A., Hong, M., Phillpot, S.R., Sinnott, S. B., 2015. An ab initio investigation of the effect of alloying elements on the elastic properties and magnetic behavior of Ni_3Al. Comput. Mater. Sci. 101, 39–46.

Ledbetter, H.M., Reed, R.P., 1973. Elastic properties of metals and alloys, I. Iron, nickel, and iron-nickel alloys, Journal of Physical and Chemical Reference Data 2 (3), 531–618.

Lejaeghere, K., Bihlmayer, G., Björkman, T., Blaha, P., Blügel, S., Blum, V., Caliste, D., Castelli, I.E., Clark, S.J., Dal Corso, A., 2016. Reproducibility in density functional theory calculations of solids. Science 351 (6280), aad3000.

Liebscher, C.H., Preußner, J., Völkl, R., Glatzel, U., 2008. Atomic site location by channelling enhanced microanalysis (ALCHEMI) in γ'-strengthened Ni-and Pt-base alloys. Acta Mater. 56 (16), 4267–4276.

Liu, S., Liu, C., Liu, W., Zhang, X., Yan, P., Wang, C., 2016. Investigation of the elemental partitioning behaviour and site preference in ternary model nickel-based superalloys by atom probe tomography and first-principles calculations. Phil. Mag. 96 (21), 2204–2218.

Lowrie, R., 1963. Elastic constants of polycrystalline MgO. Phil. Mag. 8 (95), 1965–1966.

Lu, Y., Hirohashi, M., 1999. Thermal behavior during combustion synthesis on intermetallic compound of Ni–Al system. J. Mater. Sci. Lett. 18 (5), 395–398.

Mekhrabov, A., Akdeniz, M.V., Arer, M.M., 1997. Atomic ordering characteristics of Ni_3Al intermetallics with substitutional ternary additions. Acta Mater. 45 (3), 1077–1083.

Miller, M., Jayaram, R., Lin, L., Cetel, A., 1994. APFIM characterization of single-crystal PWA 1480 nickel-base superalloy. Appl. Surf. Sci. 76, 172–176.

Miracle, D., No, O., 1993. 104 The physical and mechanical properties of NiAl. Acta Metall. Mater. 41 (3), 649–684.

Monkhorst, H.J., Pack, J.D., 1976. Special points for Brillouin-zone integrations. Phys. Rev. B 13 (12), 5188.

More, K., Miller, M., 1988. Microstructural characterization of Udimet 720: A nickel-base alloy. J. Phys. Coll. 49 (C6). C6-391–C6-396.

Murakami, H., Harada, H., Bhadeshia, H., 1994. The location of atoms in Re-and V-containing multicomponent nickel-base single-crystal superalloys. Appl. Surf. Sci. 76, 177–183.

Noebe, R.D., Bowman, R., Nathal, M.V., 1993. Physical and mechanical properties of the B2 compound NiAl. Int. Mater. Rev. 38 (4), 193–232.

Nye, J.F., 1985. Physical properties of crystals: their representation by tensors and matrices. Oxford University Press.

Özcan, S., Khmelevska, T., Khmelevskyi, S., Mohn, P., 2009. Site-preferences and local spin-polarization of transition metal solute atoms in B2 type Ni–Al alloys. Intermetallics 17 (6), 441–444.

Pal, M., Pradhan, S., Bose, P., Datta, A., Chakravorty, D., 2006. Order–disorder transition in nanocrystalline Ni_3Al prepared by a chemical route. Physica E 31 (2), 224–227.

Pan, Y., 2021. Influence of N-vacancy on the electronic and optical properties of bulk GaN from first-principles investigations. Int. J. Energy Res. 45 (10), 15512–15520.

Pan, Y., 2022. First-principles investigation of structural stability, electronic and optical properties of suboxide (Zr_3O). Mater. Sci. Eng., B 281, 115746.

Pan, Y., Chen, S., 2020. Exploring the novel structure, transportable capacity and thermodynamic properties of TiH_2 hydrogen storage material. Int. J. Energy Res. 44 (6), 4997–5007.

Pan, Y., Chen, S., 2022. Influence of alloying elements on the mechanical and thermodynamic properties of ZrB_2 boride. Vacuum 198, 110898.

Perdew, J.P., Burke, K., Ernzerhof, M., 1996. Generalized gradient approximation made simple. Phys. Rev. Lett. 77 (18), 3865.

Pettifor, D., 1992. Theoretical predictions of structure and related properties of intermetallics. Mater. Sci. Technol. 8 (4), 345–349.

Pollock, T.M., Tin, S., 2006. Nickel-based superalloys for advanced turbine engines: chemistry, microstructure and properties. J. Propul. Power 22 (2), 361–374.

Prikhodko, S., Yang, H., Ardell, A., Carnes, J., Isaak, D., 1999. Temperature and composition dependence of the elastic constants of Ni_3Al. Metallurgical and Materials Transactions A 30 (9), 2403–2408.

Pu, D., Pan, Y., 2022. First-principles investigation of solution mechanism of C in TM-Si-C matrix as the potential high-temperature ceramics. J. Am. Ceram. Soc. 105 (4), 2858–2868.

Pu, D., Pan, Y., 2022. New insight into the structural stability, ductility and melting point of Mo5SiB2 under high-pressure environment. Vacuum 196, 110727.

Pu, D., Pan, Y., 2022. First-principles investigation of oxidation mechanism of Al-doped Mo_5Si_3 silicide. Ceram. Int. 48 (8), 11518–11526.

Pu, D., Pan, Y., 2022. First-principles investigation of equilibrium phase, mechanical and thermodynamic properties of the Nowotny TM_5Si_3C ternary phase. Ceram. Int. 48 (14), 20438–20445.

Pu, D., Pan, Y., 2022. First-principles prediction of structure and mechanical properties of TM_5SiC_2 ternary silicides. Vacuum 199, 110981.

Pugh, S., Xcii., 1954. Relations between the elastic moduli and the plastic properties of polycrystalline pure metals, The London, Edinburgh, and Dublin Philosophical Magazine and Journal of. Science 45 (367), 823–843.

Raju, S., Mohandas, E., Raghunathan, V., 1996. A study of ternary element site substitution in Ni $_3$Al using pseudopotential orbital radii based structure maps. Scr. Mater. 34 (11).

Rawlings, R.D., Staton-Bevan, A.E., 1975. The alloying behaviour and mechanical properties of polycrystalline Ni_3Al (γ' phase) with ternary additions. J. Mater. Sci. 10 (3), 505–514.

Reed, R., 2006. The Superalloys. Fundamentals and Applications Cambridge Cambridge University Press 10.1017, CBO9780511541285.

Ruban, A., Skriver, H.L., 1997. Calculated site substitution in ternary γ' IH-Ni_3Al: Temperature and composition effects. Phys. Rev. B 55 (2), 856.

Saito, Y., Harada, H., 1997. The Monte Carlo simulation of ordering kinetics in Ni-base superalloys. Mater. Sci. Eng., A 223 (1–2), 1–9.

Schreiber, E., Anderson, O.L., Soga, N., Bell, J.F., 1975. Elastic constants and their measurement.

Shang, S., Wang, Y., Liu, Z.-K., 2007. First-principles elastic constants of α-and θ-Al_2O_3. Appl. Phys. Lett. 90, (10) 101909.

Shindo, D., Kikuchi, M., Hirabayashi, M., Hanada, S., Izumi, O., 1988. Site determination of Fe, Co and Cr atoms added in Ni_3Al by electron channelling enhanced microanalysis. Trans. Jpn. Inst. Met. 29 (12), 956–961.

Sluiter, M.H., Kawazoe, Y., 1995. Site preference of ternary additions in Ni_3Al. Phys. Rev. B 51 (7), 4062.

Song, Y., Guo, Z., Yang, R., Li, D., 2001. First principles study of site substitution of ternary elements in NiAl. Acta Mater. 49 (9), 1647–1654.

Stassis, C., Kayser, F., Loong, C.-K., Arch, D., 1981. Lattice dynamics of Ni_3Al. Phys. Rev. B 24 (6), 3048.

Sun, Y.J., Xiong, K., Li, Z.B., Zhang, S.M., Mao, Y., 2020. First-Principles Study of Structural, Mechanical, and Thermodynamic Properties of Refractory Metals (Rh, Ir, W, Ta, Nb, Mo, Re, and Os). Trans Tech Publ, Materials Science Forum, pp. 1017–1030.

Suzuki, T., Oya, Y., 1981. The temperature dependence of the strength of pseudo-binary platinum-based $L1_2$ alloys with B-subgroup elements. J. Mater. Sci. 16 (10), 2737–2744.

Thygesen, K.S., Jacobsen, K.W., 2016. Making the most of materials computations. Science 354 (6309), 180–181.

Togo, A., Oba, F., Tanaka, I., 2008. First-principles calculations of the ferroelastic transition between rutile-type and $CaCl_2$-type SiO_2 at high pressures. Phys. Rev. B 78, (13) 134106.

Tu, Y., Mao, Z., Seidman, D.N., 2012. Phase-partitioning and site-substitution patterns of molybdenum in a model Ni-Al-Mo superalloy: An atom-probe tomographic and first-principles study. Appl. Phys. Lett. 101, (12) 121910.

Umićević, A., Mahnke, H.-E., Belošević-Čavor, J., Cekić, B., Schumacher, G., Madjarevic, I., Koteski, V., 2016. Site preference and lattice relaxation around 4d and 5d refractory elements in Ni3Al. Journal of synchrotron radiation 23 (1), 286–292.

Wang, S.-Y., Wang, C.-Y., Sun, J.-H., Duan, W.-H., Zhao, D.-L., 2001. Energetics and electronic structure of Re and Ta in the γ' phase of Ni-based superalloys. Phys. Rev. B 65, (3) 035101.

Wang, Y.-J., Wang, C.-Y., 2009. Influence of the alloying element Re on the ideal tensile and shear strength of γ' -Ni_3Al. Scr. Mater. 61 (2), 197–200.

Wei, Z.-Y., Hu, K.-M., Sa, B.-S., Wu, B., 2021. Pressure-induced structure, electronic, thermodynamic and mechanical properties of Ti_2AlNb orthorhombic phase by first-principles calculations. Rare Met. 40 (10), 1–11.

Wei, Z., Tou, S., Wu, B., Bai, K., 2016. First principle investigation of crystal lattice structure, thermodynamics and mechanical properties in $ZnZrAl_2$ intermetallic compound. Solid State Commun. 247, 82–87.

Wojnecki, R., Lawniczak-Jablonska, K., Kachniarz, J., Perera, R., 2004. The influence of Mn atom location on the electronic structure of $Ni_3Al_{1-\ x}Mn_x$ alloys: LMTO calculation and X-ray spectroscopy. J. Alloy. Compd. 362 (1–2), 189–197.

Wu, Q., Li, S., 2012. Alloying element additions to Ni_3Al: Site preferences and effects on elastic properties from first-principles calculations. Comput. Mater. Sci. 53 (1), 436–443.

Wu, B., Zinkevich, M., Aldinger, F., Chu, M., Shen, J., 2008. Prediction of the ordering behaviours of the orthorhombic phase based on Ti_2AlNb alloys by combining thermodynamic model with ab initio calculation. Intermetallics 16 (1), 42–51.

Wu, B., Liu, H., Huang, C., Wang, M., Su, L., Zhao, C., Zhou, Z., Xiong, Y., Wu, Y., Shao, Y., 2013. Prediction of the site ordering behaviours of elements in C15 $NbCr_2$-based intermetallics by combining thermodynamic model with ab-initio calculation. Intermetallics 35, 104–109.

Wu, B., Zhao, Y., Ali, H., Chen, R., Chen, H., Wen, J., Liu, Y., Liu, L., Yang, K., Zhang, L., He, Z., Yao, Q., Zhang, H., Sa, B., Wen, C., Qiu, Y., Xiong, H., Lin, M., Liu, Y., Wang, C., Su, H., 2022. A reasonable approach to describe the atom distributions and configurational entropy in high entropy alloys based on site preference. Intermetallics 144, 107489.

Xiong, K., Gu, J., 2015. Understanding pop-in phenomena in $FeNi_3$ nanoindentation. Intermetallics 67, 111–120.

Xu, W., Han, J., Wang, Z., Wang, C., Wen, Y., Liua, X., Zhu, Z., 2013. Thermodynamic, structural and elastic properties of Co_3X (X= Ti, Ta, W, V, Al) compounds from first-principles calculations. Intermetallics 32, 303–311.

Xu, W., Shang, S., Wang, C., Gang, T., Huang, Y., Chen, L., Liu, X., Liu, Z., 2018. Accelerating exploitation of Co-Al-based superalloys from theoretical study. Mater. Des. 142, 139–148.

Yu, E., Pan, Y., 2021. Influence of noble metals on the electronic and optical properties of LiH hydride: First-principles calculations. Int. J. Hydrogen Energy 46 (71), 35342–35350.

Yu, S., Wang, C., Yu, T., 2008. The first-principles study on the doping effect of Re in Ni_3Al. Prog. Nat. Sci. 18 (7), 861–866.

Zhao, W., Sun, Z., Gong, S., 2015. Synergistic effect of co-alloying elements on site preferences and elastic properties of Ni_3Al: A first-principles study. Intermetallics 65, 75–80.

Zheng, Y., Wu, B., Zhang, C., Dai, P., 2010. Prediction of the site occupations of the ThMn12-type intermetallics $YFe_{12-x}Mo_x$ by combining thermodynamic model with ab-initio calculations. Intermetallics 18 (8), 1465–1469.

Zhou, Y., Mao, Z., Booth-Morrison, C., Seidman, D.N., 2008. The partitioning and site preference of rhenium or ruthenium in model nickel-based superalloys: An atom-probe tomographic and first-principles study. Appl. Phys. Lett. 93, (17) 171905.

Zhu, C., Yu, T., Wang, C., Wang, D., 2020. First-principles study of Ni/Ni_3Al interface doped with Re, Ta and W. Comput. Mater. Sci. 175, 109586.